


## Hafnia for analog memristor: Influence of stoichiometry and crystalline structure

Li-Heng Li , Kan-Hao Xue ,\* Jun-Hui Yuan, Ge-Qi Mao, and Xiangshui Miao

*School of Integrated Circuits, School of Optical and Electronic Information, Huazhong University of Science and Technology, Wuhan 430074, China*

*and Hubei Yangtze Memory Laboratories, Wuhan 430205, China*



(Received 14 April 2022; accepted 28 July 2022; published 25 August 2022)

The highly nonlinear switching behavior of hafnia memristor actually hinders its wide application in neuromorphic computing. The theoretical understanding of its switching mechanism has been focused on the processes of conductive filament (CF) generation and rupture, but the possible phase transition and crystallization around the region of CFs due to the variation of O content have been less studied or understood. In this paper,  $\text{HfO}_x$  structural models covering the full stoichiometries from Hf to  $\text{HfO}_2$  are established, and the crystal structure evolution during the reduction process of hafnia is obtained through first-principles calculation. The electronic structures and O vacancy migration characteristics of these structures are analyzed. A criterion is prescribed to predict the mode of abrupt binary switching or gradual conductance modulation according to the structure evolution of the CFs. In particular, factors that influence the merging of tiny conductive channels into strong CFs are discussed intensively, including the anisotropy of O vacancy migration and the size effect. The feasibility of Mg doping to achieve robust gradual switching is discussed.

DOI: [10.1103/PhysRevMaterials.6.084603](https://doi.org/10.1103/PhysRevMaterials.6.084603)

### I. INTRODUCTION

Due to their high speed, complementary metal-oxide semiconductor (CMOS)-compatible nature, and three-dimensional (3D) integration potential [1–4], binary oxide memristors have been widely used in nonvolatile data storage, logic computing, and neuromorphic computing [5–12]. In particular, hafnia ( $\text{HfO}_2$ )-based memristors attract a great deal of attention due to their downscale potential, nanosecond-level erasing time, and excellent data retention [13–16]. Moreover, the resistive switching (RS) window of hafnia memristors is typically higher than other binary oxides such as  $\text{TaO}_x$  and  $\text{TiO}_x$  [17–21], favoring their application as binary data storage. The capability of establishing a robust Schottky barrier between the conductive filaments (CFs) and  $\text{HfO}_2$  has been revealed to account for such a large RS window [22]. However, the actual application scenario may require different RS characteristics. For the sake of neuromorphic computing, linearity and symmetry are key aspects for the analog RS of the memristor [23]. In general, its highly nonlinear RS behavior hinders the application of hafnia-based memristor in neuromorphic computing [24,25]. Element doping and combined use with other RS materials are possible solutions, but there is still no well-established theory to overcome the abrupt RS behaviors in  $\text{HfO}_2$ .

To fundamentally resolve this problem, it is necessary to gain a deeper and material-specific understanding of the RS mechanism of an  $\text{HfO}_2$ -based memristor. While the commonly accepted RS picture in  $\text{HfO}_2$ -based memristors is the formation and rupture of O-deficient CFs [26,27], exciting new discoveries have been made in the past few years. Celano *et al.* directly observed the conical structure of CFs

in an Hf/ $\text{HfO}_2$ /TiN memristor through their newly designed scalpel-SPM (scanning probe microscopy) technique, which is a kind of conductive atomic force microscopy, and they defined the CF as a local region populated with O vacancies ( $V_O$ 's) [28]. The cross-sectional area of a typical CF in their experiment was  $\sim 40 \text{ nm}^2$  at the active Hf electrode size but merely  $\sim 10 \text{ nm}^2$  at the more inert TiN electrode side. Therefore,  $V_O$ 's diffuse and migrate from the active electrode side toward the inert electrode side during the formation of CFs. Although the exact composition/stoichiometry of the CF was not obtained, that work has lent strong support to the  $V_O$ -induced CF conduction in hafnia memristors. Kumar *et al.* observed that the CF in hafnia consists of an O-poor conductive core surrounded by an O-rich region [29]. The formation and dissolution of the CFs were ascribed to the radial thermophoresis and Fickian diffusion of O atoms driven by Joule heating. The role of O migration and its induced electrochemical reactions were further probed directly by Yang *et al.* in  $\text{HfO}_2$  and  $\text{TaO}_x$  memristors with a spherical aberration (Cs)-corrected transmission electron microscope (TEM) [30]. In 2018, Yin *et al.* [31] showed high-resolution TEM (HRTEM) evidence that the CFs in hafnia memristors consist of crystalline regions of monoclinic and orthorhombic symmetry, even though the pristine hafnia film was amorphous before electroforming. The work indicates the significance of crystalline  $\text{HfO}_x$  phases for the search of CF structure in amorphous hafnia-based memristors. For polycrystalline hafnia films, it has been shown that the CFs prefer to emerge near grain boundaries [32] where the creation of  $V_O$ 's can be easier than in the bulk [33].

Very recently, Zhang *et al.* [34] identified the crystalline structure of the CFs in hafnia memristors through comprehensive HRTEM imaging for Pt/ $\text{HfO}_2$ /Pt, TiN/ $\text{HfO}_2$ /Pt, Ta/ $\text{HfO}_2$ /Pt, Hf/ $\text{HfO}_2$ /Pt, and Ti/ $\text{HfO}_2$ /Pt cells. The CF consists of a hexagonal  $\text{Hf}_6\text{O}$  metal core surrounded by an O-rich

\*Corresponding author: xkh@hust.edu.cn

monoclinic  $\text{HfO}_x$  ( $m\text{-HfO}_x$ ) or tetragonal  $\text{HfO}_x$  ( $t\text{-HfO}_x$ ) shell. The crystalline feature of the CFs is very prominent, though the pristine hafnia thin films were always amorphous. In that work, the electroforming and SET/RESET operations were sufficiently thorough to support a  $10^6$  RS window, thus the core-shell CF structure has exactly been confirmed at least for the binary RS mode of hafnia memristors. The observation of the thermodynamically stable  $\text{Hf}_6\text{O}$  phase (i.e.,  $\sim\text{HfO}_{0.17}$ ) is also consistent with the theoretical prediction by McKenna ( $\text{HfO}_{0.2}$ ) [35] through an energetic argument.

Notwithstanding these new discoveries, including concrete TEM evidence, it must be emphasized that to identify the CF of hafnia memristors under gradual switching mode (or say, working as an analog memristor) through TEM is much more difficult than under the binary switching mode. A gradual resistance modulation may not alter the symmetry of the CF, but it only involves mild ionic migration. The conductivity variation among different regions is also expected to be much slighter than the binary mode. Since the gradual RS mode is very important for neuromorphic computing applications, theoretical calculations become a viable choice. In particular, the previous discovery that the CF involves crystalline regions could greatly facilitate the theoretical investigation of the CF composition and structure in hafnia memristors under the gradual RS mode. Using first-principles calculations, the RS mechanism in hafnia has been studied intensively. Perevalov and Islamov *et al.* used first-principles calculations to simulate the electronic structures of various defects in  $\text{HfO}_2$ , including the  $\text{V}_\text{O}$ , interstitial O, interstitial Hf, as well as Hf substituting for O, and they showed that  $\text{V}_\text{O}$ 's are the key defects for the charge transport and resistive random access memory (RRAM) operability [36], verifying the importance of  $\text{V}_\text{O}$  in the RS process. The theoretical study of the formation and migration of  $\text{V}_\text{O}$  shows that there is an optimal path with low migration barrier [37], which is beneficial to the reduction of operating voltage and the acceleration of the signal response. However, a low migration barrier also leads to poor thermal stability of hafnia-based memristors [38]. Several works have shown the tendency of O vacancy clustering in hafnia [39,40], which explains the formation of conical structure CFs in  $\text{HfO}_2$  and confirms a size limit of CFs in Hf or Hf-like compositions ( $\sim 0.4 \text{ nm}^2$ ) [40].

These previous theoretical studies, however, did not cover all possible crystalline  $\text{HfO}_x$  phases between Hf and  $\text{HfO}_2$ . Most works emphasize the significance of  $\text{V}_\text{O}$  concentration for conduction, but the resulting phases with sufficient  $\text{V}_\text{O}$  concentration that act as CFs are unclear. On account of the experimental identification of crystalline CF structures, various  $\text{HfO}_x$  ( $0 \leq x < 2$ ) phases ought to be examined for possible CF composition of hafnia memristors under the gradual RS mode. Actually, a number of Hf suboxide phases have been either predicted or discovered. Some well-known hexagonal ( $h$ -) phases can be regarded as the derivatives of hcp Hf, including  $h\text{-Hf}_6\text{O}$  ( $R\bar{3}$ ),  $h\text{-Hf}_3\text{O}$  ( $R\bar{3}c$ ), and  $h\text{-Hf}_2\text{O}$  ( $P\bar{3}1m$ ) [41]. The ground state of HfO has been predicted to be tetragonal ( $t$ -)  $I4_1/amd$ , which is metallic and has also been extensively observed in the experiments by Zhang *et al.* [34]. Ground-state ZrO, however, was predicted to possess a  $P\bar{6}2m$  structure [42]. Its  $h\text{-HfO}$  counterpart is energetically less favorable than  $t\text{-HfO}$ , and surprisingly shows a tiny band

gap [43]. Predicted  $\text{Hf}_2\text{O}_3$  phases involve a tetragonal  $P\bar{4}m2$  structure [44] and an orthorhombic  $Ibam$  structure [45], with the former slightly lower in energy. Several other pressure-induced  $\text{HfO}_x$  suboxides have also been predicted [41]. The sequence of suboxide presence during the reduction of  $\text{HfO}_2$  has been summarized as roughly from the tetragonal symmetry to the hexagonal symmetry [46]. A recent work shows that the transitional stoichiometry is around  $\text{HfO}_{0.7}$  [47].

In hafnia memristors, the reduction of  $\text{HfO}_2$  is limited to a directional electric field and thermal forces, which is different from the reduction in bulk forms. We shall establish the relation among various  $\text{HfO}_x$  phases in memristor applications. Based on the comprehensive materials information, we then derive the working modes of hafnia memristors. The size-composition relation of CFs in hafnia will also be investigated.

## II. MODELING AND COMPUTATIONAL DETAILS

### A. General considerations

At atmospheric pressure and low temperature, monoclinic  $P2_1/c$  is the most stable phase of  $\text{HfO}_2$ , which can stand up to  $\sim 2000$  K [48], thus becoming the natural choice of our starting point for the pristine state of  $\text{HfO}_2$ -based devices. As only the CFs and their surrounding regions are significant, which account for the RS behaviors, such a crystalline starting point also makes sense for the initially amorphous  $\text{HfO}_2$  memristors. There is concrete experimental evidence that the CF-surroundings can be crystallized through the Joule heating effect from electroforming, SET, and RESET operations [34]. Therefore, we gradually increased the oxygen vacancy concentration in  $m\text{-HfO}_2$ , covering the full stoichiometries from  $\text{HfO}_2$  to Hf. After structural optimization, these reduced  $\text{HfO}_x$  models could give useful information regarding the relatively stable  $\text{HfO}_x$  structures for  $0 < x < 2$ , which can possibly be metastable from thermodynamics but are more favorable against other structures at that specific stoichiometry. Moreover, ion migration barriers were systematically calculated to explore the possible transition routes between these stable or metastable phases. The kinetic information is highly relevant because our primary concern is the scenario of memristor application, where only a unidirectional (either positive or negative) electric field is applied to the capacitor. In this case, some thermodynamically favorable phases may not be reached due to high transitional barriers.

### B. Modeling details

The structure of  $m\text{-HfO}_2$  is illustrated in Fig. 1, which derives from the cubic fluorite structure, but the Hf coordination has been reduced from 8 to 7 in terms of the monoclinic distortion. There are two inequivalent O sites, 3-coordination O(A1-A4) and 4-coordination O(B1-B4). The O-atom layer including O(B1), O(B2), O(A3), and O(A4) is equivalent to the layer including O(A1), O(A2), O(B3), and O(B4). A specific amount of O atoms (from 1 to 8) was removed from the 12-atom primitive cell  $\text{Hf}_4\text{O}_8$ , and the remaining structure was subject to full relaxation. Of course, we cannot start from all possible  $m\text{-HfO}_2$  supercells for O removal, which is an endless task. Nevertheless, previous experience shows that the

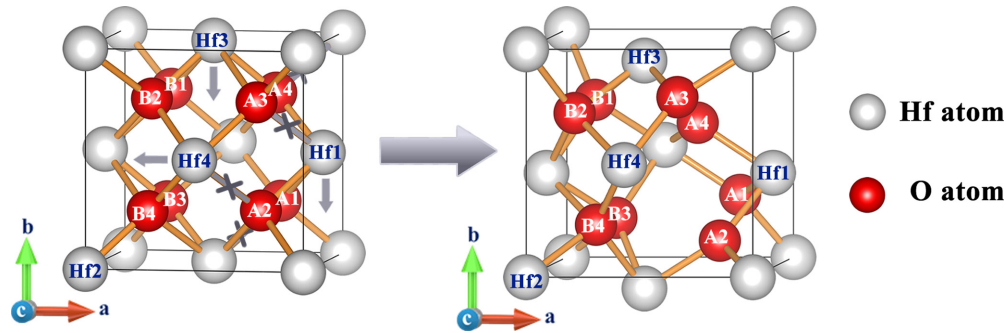


FIG. 1. The structure of  $m\text{-HfO}_2$  (right) as derived from the cubic fluorite structure (left). The basic directions of Hf movement and the broken Hf-O bonds are marked for the monoclinic distortion.

$\text{Hf}_4\text{O}_8$  primitive cell is sufficiently large to yield possible suboxide phases [44]. Moreover, we shall show that all reported or predicted  $\text{HfO}_x$  cases are included in or related to our search results, which proves the effectiveness of the method *a posteriori*. Careful symmetry analysis has eliminated a number of redundant cases, ending up with only 32 inequivalent  $\text{HfO}_x$  models, as summarized in Fig. 2.

### C. Computational details

The *ab initio* calculations were carried out using density functional theory (DFT) [49,50] as implemented in the plane-wave based Vienna *Ab initio* Simulation Package (VASP 5.4.4) [51,52]. The generalized gradient approximation (GGA) was adopted for the exchange-correlation energy, in the Perdew-Burke-Ernzerhof functional form [53]. It is well known that DFT-GGA systematically underestimates the band gaps for semiconductors and insulators. Hence, we implemented an efficient self-energy correction scheme (DFT-1/2) [54–56], originally proposed by Ferreira *et al.* and later improved by Xue *et al.* (shDFT-1/2) [57], to carry out electronic structure calculation. Both the electronic structure and the  $\text{V}_\text{O}$  migration barrier were calculated based on  $2 \times 2 \times 2$  (96-atom) supercells (see Note 1 in the Supplemental Material [58] for detailed calculation parameter settings). The migration barrier was calculated using a climbing image nudged elastic band (CI-NEB) method.

## III. RESULTS AND DISCUSSION

### A. Structural analysis of $\text{HfO}_x$ at various stoichiometries

For structural optimization of the 32 primitive cell models, high-precision full relaxation was carried out first. To visualize the changes of crystal structures, the relaxation results were extended to  $2 \times 2 \times 2$  supercell structures, as illustrated in Fig. 3. On the other hand, Fig. 4 summarizes the possible  $\text{HfO}_x$  structures under various stoichiometries, which may be classified into three regimes.

Regime 1 ( $1.5 < x \leq 2.0$ ): All  $\text{HfO}_x$  structures in this regime remain in the monoclinic symmetry ( $m\text{-HfO}_x$ ), including Case-2 and Case-3.

Regime 2 ( $1.0 \leq x \leq 1.5$ ): There are both monoclinic phases ( $m\text{-HfO}_x$ : Case-4, Case-5, Case-7, and Case-9) and tetragonal phases ( $t\text{-HfO}_x$ : Case-6 and Case-8). The binding energies of  $m\text{-HfO}_x$  structures are between  $-7.58$  eV/f.u. (f.u.

stands for a formula unit) and  $-7.70$  eV/f.u. (see Note 2 in the Supplemental Material [58]), where the lowest-energy structure is Case-4, which will subsequently be intensively analyzed as the prototype  $m\text{-HfO}_{1.5}$  structure. The  $t\text{-HfO}_x$  structure is shown in Fig. 4(b), where Hf atoms maintain an fcc-like structure (though distorted) and O atoms can occupy two types of positions (Site-1 and Site-2). When all O atoms occupy Site-1, the structure is the  $P2/c\text{-HfO}_{1.5}$  phase (Case-8). Provided that O atoms occupy both Site-1 and Site-2, a  $P4m2\text{-HfO}_{1.5}$  phase (Case-6) can then be recovered. The obtained  $\text{HfO}_{1.25}$  structures are similar to that of  $\text{HfO}_{1.5}$ , and they can also be divided into  $m\text{-HfO}_x$  (Case-12) and  $t\text{-HfO}_x$  (Case-10 and Case-11).

Regime 3 ( $x < 1.0$ ): There are a variety of phase structures in this regime, but in all cases the Hf atoms remain in quasi-fcc structure and the O atoms occupy Site-1 or Site-2 positions. Therefore, these structures can be regarded as O-deficient structures of  $t\text{-HfO}_2$  and  $P4m2\text{-HfO}_{1.5}$ .

However, no known  $h\text{-HfO}_x$  structure was obtained through this modeling method. This is due to the constriction of the Hf-subsystem topology, which fails to be converted to hexagonal symmetry. Previous studies [41,45] have demonstrated the vicinity of pure Hf in the Hf-O system, where the hcp structure is preserved and the extra content of O is distributed among the interstitial positions octahedrally coordinated by Hf atoms. It has also been confirmed experimentally that  $\text{HfO}_x$  will be converted into  $h\text{-HfO}_x$  at  $x = 0.7$  [47]. Theoretically, the O content of  $h\text{-HfO}_x$  can reach  $x = 0.83$ , and the corresponding structure is  $h\text{-Hf}_6\text{O}_5$ , as shown in Fig. 4(c). Therefore, the  $\text{HfO}_x$  structure in Regime 3 ( $x < 1.0$ ) is considered to be  $h\text{-HfO}_x$ . Our method thus covers the O-rich phases prior to the tetragonal-to-hexagonal transition.

Obviously,  $\text{HfO}_2$  underwent a transition from the monoclinic phase to tetragonal phases, and eventually to hexagonal symmetry upon decreasing the O content. A critical stoichiometry is discovered to be  $x = 1.5$ , at which there are three phases,  $m\text{-HfO}_{1.5}$ ,  $P4m2\text{-HfO}_{1.5}$  (hereafter named  $\alpha\text{-HfO}_{1.5}$  or  $\alpha\text{-Hf}_2\text{O}_3$ ), and another tetragonal phase of  $\text{HfO}_{1.5}$  derived from  $P4_2/nmc\text{-HfO}_2$ . Their crystal structures are illustrated in Fig. 3 as Case-1, Case-6, and Case-8. Another predicted  $Ibam$  phase of  $\text{HfO}_{1.5}$  (referred to as  $\beta\text{-HfO}_{1.5}$  or  $\beta\text{-Hf}_2\text{O}_3$  for convenience) [45] is not included in Fig. 3, but its relation to other  $\text{HfO}_x$  phases will be clear soon. The tetragonal phase of  $\text{HfO}_{1.5}$  derived from  $P4_2/nmc\text{-HfO}_2$  has a  $P2/c$  symmetry, and it will be referred to as  $\gamma\text{-HfO}_{1.5}$  in this work. Figure 5(a)

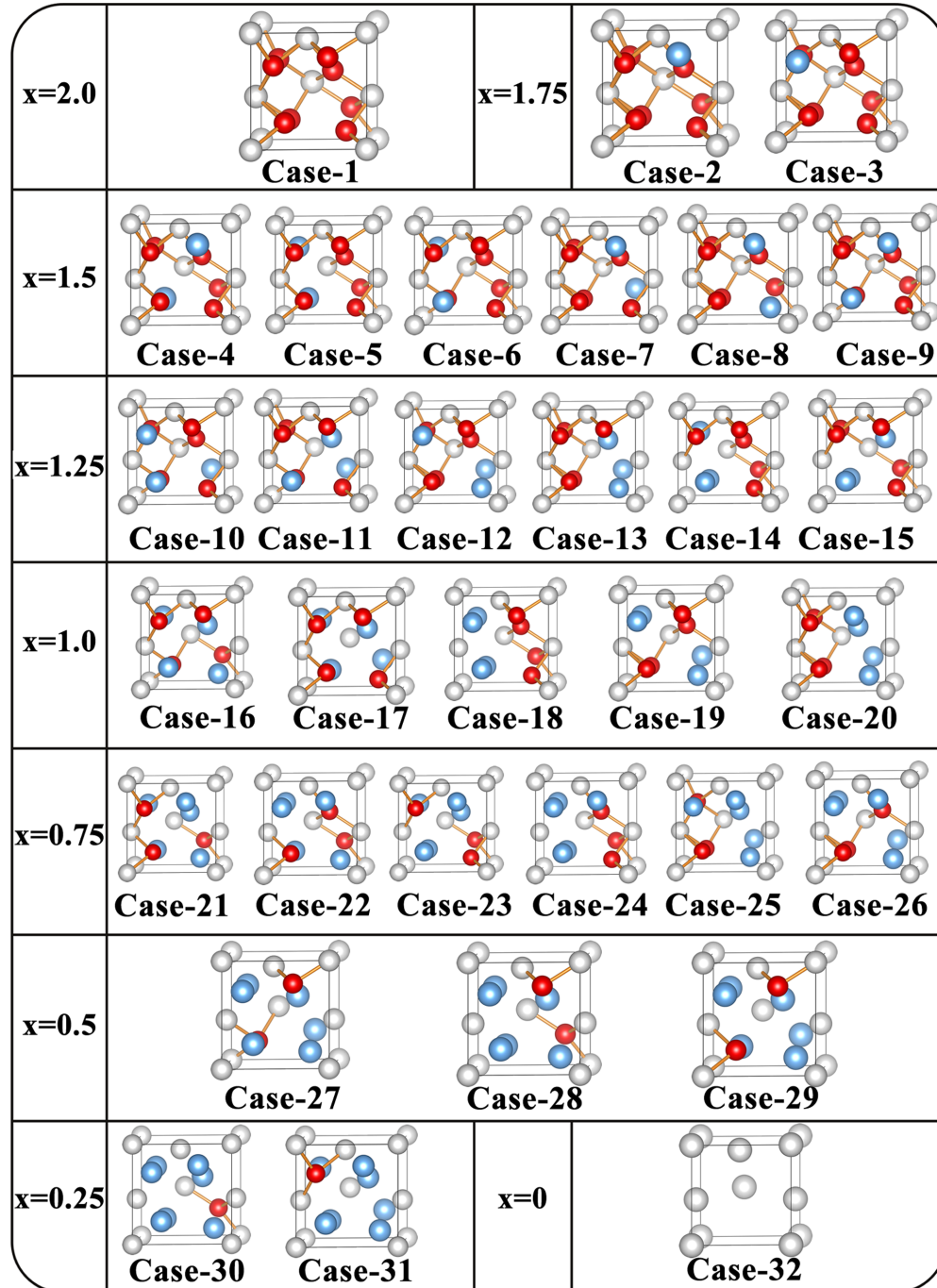


FIG. 2. The 32 inequivalent unit-cell models of the full range of Hf-O binary compounds in our search. Red balls stand for O atoms, blue balls represent  $V_O$ , and white balls correspond to Hf atoms.

shows their Helmholtz free energy variations with respect to temperature  $T$ , with the vibrational entropies calculated using the harmonic-oscillator model (details given in Note 3 of the Supplemental Material [58]). Zero-point energy was added to the free energy for  $T = 0$  K in each phase. With the lowest free energy at zero temperature,  $\alpha$ -HfO<sub>1.5</sub> is used as a reference. The results show that the phase-transition temperature between  $m$ -HfO<sub>1.5</sub> and  $\alpha$ -HfO<sub>1.5</sub> is 2490 K, and that between  $\alpha$ -HfO<sub>1.5</sub> and  $\gamma$ -HfO<sub>1.5</sub> is 1193 K. These high temperatures can hardly be obtained during the memristor operations. In other words, reversible phase transition between

$\alpha$ -HfO<sub>1.5</sub> and the other two phases is unlikely through Joule heating. Nevertheless, the phase transition between  $\gamma$ -HfO<sub>1.5</sub> and  $m$ -HfO<sub>1.5</sub> can occur at merely 62 K. This is a remarkable result, since the phase-transition temperature between  $t$ -HfO<sub>2</sub> and  $m$ -HfO<sub>2</sub> is well known to be as high as 1973 K [48]. Hence, the existence of abundant O vacancies improves the stability of  $P4_2/nmc$ -like HfO <sub>$x$</sub>  [34]. It also implies that a CF with  $m$ -HfO<sub>1.5</sub> structure would spontaneously transform into the  $\gamma$ -HfO<sub>1.5</sub> structure.

A different Hf<sub>2</sub>O<sub>3</sub> phase with the  $Ibam$  symmetry (i.e.,  $\beta$ -HfO<sub>1.5</sub> in this work) was predicted by Rushchanskii *et al.*

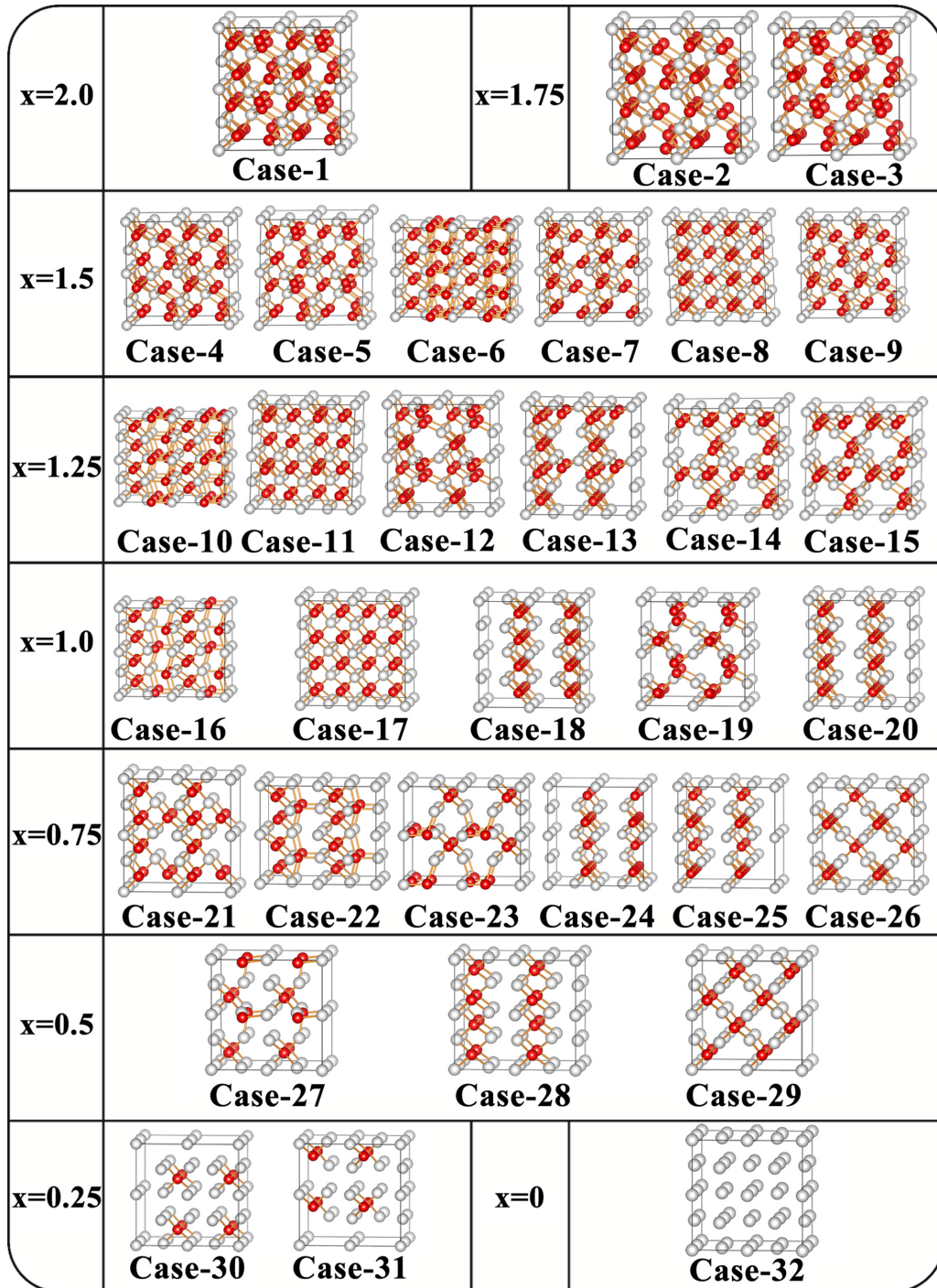


FIG. 3. Structural demonstration of the 32 inequivalent models after complete relaxation.

in 2018 [45]. Figures 6(a) and 6(b) compare the atomic structures of  $\beta$ -HfO<sub>1.5</sub> and  $\gamma$ -HfO<sub>1.5</sub>. Their topological structures are extremely similar. Actually,  $\beta$ -HfO<sub>1.5</sub> is obtained by introducing *b*-direction V<sub>O</sub> chains in cubic HfO<sub>2</sub> (*c*-HfO<sub>2</sub>), while  $\gamma$ -HfO<sub>1.5</sub> is derived through the same procedure, but starting from *t*-HfO<sub>2</sub>. Therefore, O anions are strictly aligned along the *b*-direction in  $\beta$ -HfO<sub>1.5</sub>, but a zigzag sequence of O anions is observed in  $\gamma$ -HfO<sub>1.5</sub>. Our calculation roughly shows a critical temperature of 544 K for their phase transition. Hence,  $\beta$ -HfO<sub>1.5</sub> may be obtained from  $\gamma$ -HfO<sub>1.5</sub> at a finite temperature.

Besides  $x = 1.5$ , another important stoichiometry during the reduction process of hafnia is  $x = 1$ , where the lowest-energy HfO phase is  $I4_1/amd$ -HfO as predicted by Zhu *et al.* [59] [structure shown in Fig. 6(c), with the unit cell rotated by 45° along the *c*-axis to be better compared with the other HfO phase]. It will be called  $\alpha$ -HfO for convenience, while  $\beta$ -HfO refers to the  $P\bar{6}2m$  phase [42,43]. Moreover, HfO may also be obtained through introducing more O vacancies from  $\gamma$ -HfO<sub>1.5</sub>, yielding the tetragonal  $\gamma$ -HfO phase in a  $P4_2/mmc$  space group, as illustrated in Figs. 6(b) and 6(d). The free-energy comparison for these HfO phases is given

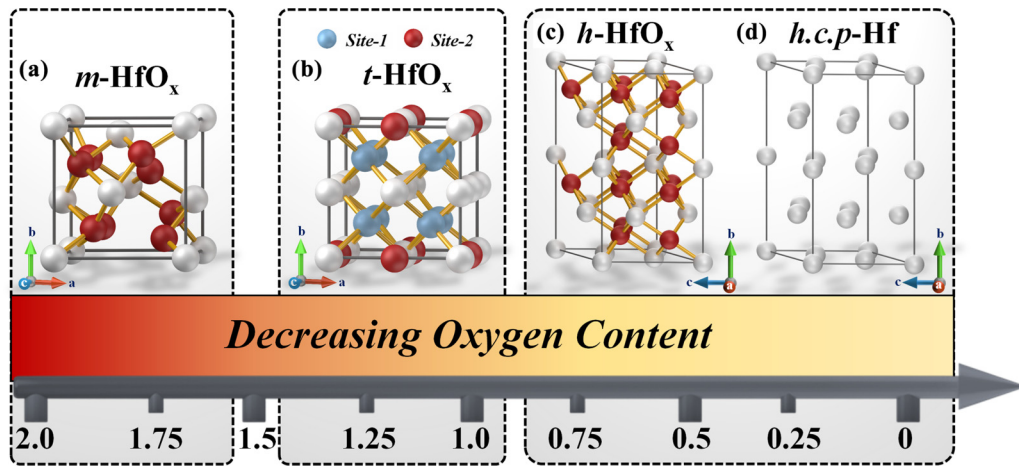


FIG. 4. The phase structure evolution of  $\text{HfO}_x$  during the reduction process.

in Fig. 5(b). Although the ground-state total energy calculation favors  $\alpha$ -HfO, after considering the zero-point energy,  $\beta$ -HfO becomes the most favorable phase at zero temperature. The phase-transition temperature between  $\alpha$ -HfO and  $\beta$ -HfO ( $\gamma$ -HfO) is 216 K (152 K). Hence,  $\beta$ -HfO and  $\gamma$ -HfO may be converted to  $\alpha$ -HfO at room temperature.

**B. Relations between  $\text{HfO}_2$  and several Hf suboxides**

The Hf suboxides with tetragonal or orthorhombic symmetries are all metastable at room temperature and atmospheric pressure, according to thermodynamic data [41]. However, they may be stabilized in a memristor device due to mechanical confinement and/or under a certain stress. In memristors, the special situation is that these phases should be derived during the reduction process of  $\text{HfO}_2$ , mainly within the electroforming step. Therefore, before exploring the possibility of a suboxide to serve as the CF, it is a prerequisite to understand its relation to  $m$ - $\text{HfO}_2$ , or to fluorite  $c$ - $\text{HfO}_2$ , because  $m$ - $\text{HfO}_2$  can be regarded as a distorted version of the fluorite structure.

To this end, we first note that it is the topology of the Hf subsystem that determines whether  $\text{HfO}_x$  is in a tetragonal-like structure or a hexagonal structure. The Hf-subsystem is fcc or distorted fcc for the former, but it becomes hcp for the latter. The O anions may reside near the eight fluorite sites (Site-1) or near the four rocksalt sites

(Site-2). Although  $m$ - $\text{HfO}_2$  is highly distorted, all its O anions still reside at Site-1, as in the fluorite structure. The monoclinic distortion reduced the Hf coordination number to 7, which better fits the ionic radius ratio between  $\text{Hf}^{4+}$  and  $\text{O}^{2-}$  [60]. As  $x$  becomes 1.5, neither the fluorite structure nor the rocksalt structure fits its stoichiometry, but their 1:1 mixture does. Hence,  $\alpha$ - $\text{HfO}_{1.5}$  is in fact a natural candidate, which can be viewed as removing half of the 4-coordination O anions from  $m$ - $\text{HfO}_2$ , followed by transferring the 3-coordination O anions from Site-1 to Site-2, as illustrated in Figs. 7(a)–7(d). The Site-2 O anions show a further distortion along the  $c$ -axis, which renders 7-coordination for the Hf cations instead of 8. On the other hand, both  $\beta$ - $\text{HfO}_{1.5}$  and  $\gamma$ - $\text{HfO}_{1.5}$  only require creating  $\text{V}_\text{O}$  chains along the  $b$ -axis of  $m$ - $\text{HfO}_2$ , without interchanging Site-1 and Site-2 O anions, as illustrated in Figs. 7(e)–7(g). Actually, they possess no Site-2 O anions, just like in  $m$ - $\text{HfO}_2$  and  $t$ - $\text{HfO}_2$ .

When it comes to HfO, we first notice that  $\gamma$ -HfO is closely related to  $\gamma$ - $\text{HfO}_{1.5}$  through simply introducing more  $\text{V}_\text{O}$ 's. At  $x = 1.0$ ,  $\gamma$ -HfO becomes much more symmetric ( $P4_2/mmc$ ) than  $\gamma$ - $\text{HfO}_{1.5}$  ( $P2/c$ ). On the other hand,  $\alpha$ -HfO could also be derived from  $\gamma$ - $\text{HfO}_{1.5}$ , with more  $\text{V}_\text{O}$  chains introduced. Figures 6(c) and 6(d) show that the structures of  $\alpha$ -HfO and  $\gamma$ -HfO are highly similar. The Hf and O atoms in  $\alpha$ -HfO have been slightly distorted compared with  $\gamma$ -HfO, but the global Hf-sublattice is still of fcc-type and all O atoms reside at

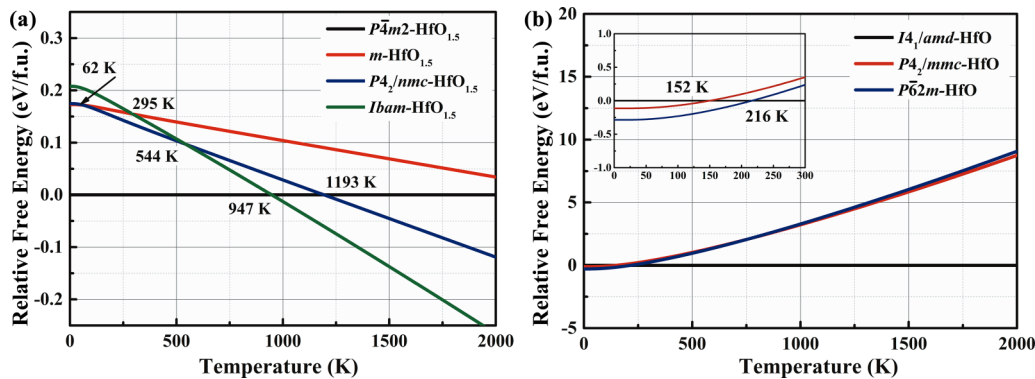


FIG. 5. Relative Helmholtz free energies of (a)  $m$ - $\text{HfO}_{1.5}$ ,  $P2/c$ - $\text{HfO}_{1.5}$ , and  $P4m2$ - $\text{HfO}_{1.5}$ ; (b)  $I4_1/amd$ -HfO,  $P4_2/mmc$ -HfO, and  $P6_2m$ -HfO. The free energy of a selected phase ( $P4m2$ - $\text{HfO}_{1.5}$  or  $I4_1/amd$ -HfO) is set to zero at any temperature.

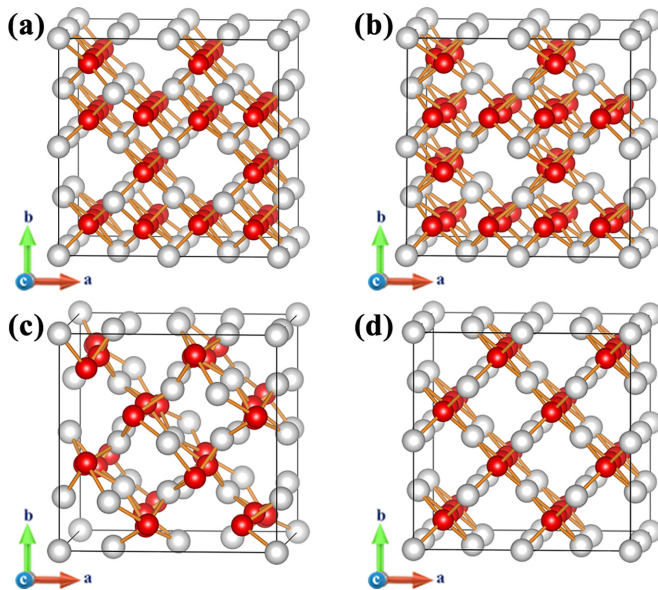


FIG. 6. The structure diagrams of (a) *Ibam*- $\text{HfO}_{1.5}$  ( $\beta$ - $\text{HfO}_{1.5}$ ), (b) *P2/c*- $\text{HfO}_{1.5}$  ( $\gamma$ - $\text{HfO}_{1.5}$ ), (c) *I41/amd*- $\text{HfO}$  ( $\alpha$ - $\text{HfO}$ ), and (d) *P42/mmc*- $\text{HfO}$  ( $\gamma$ - $\text{HfO}$ ).

Site-1. Such tiny distortion reduces the free energy, rendering  $\alpha$ - $\text{HfO}$  more stable than  $\gamma$ - $\text{HfO}$  at room temperature. Note that in all predicted and experimentally observed  $\text{HfO}$  phases, the O atoms occupy Site-1 rather than Site-2. As  $\alpha$ - $\text{HfO}_{1.5}$  requires a partial occupation of Site-2, the rule observed in  $\text{HfO}$  confirms that  $\alpha$ - $\text{HfO}_{1.5}$  is a bit isolated from the global path of hafnia reduction under the memristor situation, though the direct growth of  $\text{HfO}_x$  under O-poor condition may yield  $\alpha$ - $\text{HfO}_{1.5}$  [61,62].

If the fcc-sublattice for Hf is to be maintained, the prototype models with O occupying Site-1 and Site-2 are *c*- $\text{HfO}_2$  and rocksalt  $\text{HfO}$ , respectively. Their mixture generates  $\text{HfO}_x$  with  $1 < x < 2$ . The rocksalt structure is indeed a simple potential phase for  $\text{HfO}$ , where the O atoms may only occupy Site-2. However, in addition to its high energy, the phonon spectra of rocksalt  $\text{HfO}$  show that it is kinetically unstable. The Hf-O bond length in rocksalt  $\text{HfO}$  is also longer than in  $\alpha$ -,  $\beta$ -, and  $\gamma$ -phases of  $\text{HfO}$ , but it is more ionic than other phases. Detailed comparisons and calculation data for rocksalt  $\text{HfO}$  are presented in Note 4 of the Supplemental Material [58].

The next issue is the structure of  $\text{HfO}_x$  with  $x < 1$ . The kinetic instability of rocksalt  $\text{HfO}$  hinders the formation of cubic like  $\text{HfO}_x$  ( $x < 1$ ) by introducing  $\text{V}_\text{O}$ 's from rocksalt  $\text{HfO}$ . However, introducing  $\text{V}_\text{O}$ 's in  $\gamma$ - $\text{HfO}$  or  $\alpha$ - $\text{HfO}$  (which is almost the same) is a possible route. We therefore obtained  $\gamma$ - $\text{HfO}_{0.75}$ , but its phonon instability (see Note 5 of the Supplemental Material [58]) indicates that keeping the fcc-like Hf-sublattice is no longer feasible for highly reduced Hf suboxides with  $x < 1$ . Hence, a major structural change from fcc-Hf to hcp-Hf inevitably occurs near the stoichiometry of  $\text{HfO}$ . The experimentally observed transition stoichiometry at  $\sim\text{HfO}_{0.7}$  [47] is not far away. If starting from the hcp-Hf sublattice side, the possible emergence of hexagonal  $\beta$ - $\text{HfO}$  through backward oxidation still cannot be ruled out. To sum

up, the relation between various Hf-O compounds during the reduction process of  $\text{HfO}_2$  is given in Fig. 8.

### C. The electrical and $\text{V}_\text{O}$ migration properties in different $\text{HfO}_x$ phases

There are two reasons to understand the modes and difficulty of  $\text{V}_\text{O}$  migration in these  $\text{HfO}_x$  phases. On the one hand, it helps to determine whether a specific  $\text{HfO}_x$  suboxide phase may be obtained starting from  $\text{HfO}_2$  (either amorphous or polycrystalline), under the memristor operation conditions. This adds to our understanding of the CF formation from a kinetic point of view, besides the thermodynamic point of view. On the other hand, technically favorable CFs should possess proper migration barriers for  $\text{V}_\text{O}$ 's, since too low barriers could deteriorate the stability of CFs as well as the device retention, but too high barriers would increase the device operation voltage.

#### 1. Transition barriers between various $\text{HfO}_x$ phases

To understand which suboxide phases are likely to emerge during the reduction process of hafnia, we set up a  $2 \times 2 \times 2$  supercell for *m*- $\text{HfO}_2$  to investigate the migration barriers of O vacancies, along  $\text{B4} \rightarrow \text{B1}$  (for the sake of  $\alpha$ - $\text{HfO}_{1.5}$  formation) as well as  $\text{A2} \rightarrow \text{A3}$  (for the sake of  $\gamma$ - $\text{HfO}_{1.5}$  formation) paths, considering both neutral  $\text{V}_\text{O}$  and  $\text{V}_\text{O}^{2+}$ . These paths are self-continuous so as to enable drastic phase transitions. As illustrated in Fig. 9, the migration barriers for  $\text{V}_\text{O}$  and  $\text{V}_\text{O}^{2+}$  are similar along the  $\text{B4} \rightarrow \text{B1}$  path, as high as  $\sim 5.0$  eV. Yet, for the  $\text{A2} \rightarrow \text{A3}$  path, migration barriers for  $\text{V}_\text{O}^{2+}$  and neutral  $\text{V}_\text{O}$  are merely 2.39 and 2.98 eV, respectively. Hence, under the driving force of electric field, it is easier to obtain  $\gamma$ - $\text{HfO}_{1.5}$  rather than  $\alpha$ - $\text{HfO}_{1.5}$  from a kinetic point of view. On the other hand, to derive  $\alpha$ - $\text{HfO}_{1.5}$  from  $\gamma$ - $\text{HfO}_{1.5}$ , a part of the O atoms have to migrate from Site-1 to Site-2, whose transition barrier is larger than the migration from Site-1 to Site-1 (details are shown in Sec. III C 2). Accordingly, the  $\text{HfO}_x$  CF with  $1.0 < x < 1.5$  tends to keep the tetragonal symmetry as in  $\gamma$ - $\text{HfO}_x$ .

#### 2. RS within *m*- $\text{HfO}_x$

As mentioned in Sec. III A, when the Hf/O ratio  $x$  is greater than 1.5, the single-phase  $\text{HfO}_x$  crystal structure remains monoclinic. For such a range of stoichiometry, the structures and density of states of *m*- $\text{HfO}_x$  are shown in Fig. 10, confirming their semiconductor characteristic for the entire range  $1.5 < x < 2.0$ . Provided that *m*- $\text{HfO}_x$  is to serve as the conductive channel, the RS will be confined to the high resistance state (HRS), but resistance modulation within a limited range (compared with the binary RS mode) is still possible. A potential benefit of this mode lies in the fact that no sharp transition to a metallic state is involved, therefore the linearity of the RS may become better. Indeed, as the O content decreases, the defect states in *m*- $\text{HfO}_x$  get stronger and accumulate below the conduction-band minimum (CBM), lowering the energy gap to a value of 0.24 eV at  $x = 1.5$ . The reduced defect excitation barrier should render much more excited carriers and improve the conductivity of *m*- $\text{HfO}_x$ . The HRS of hafnia-based memristors may vary dramatically with O content. Our

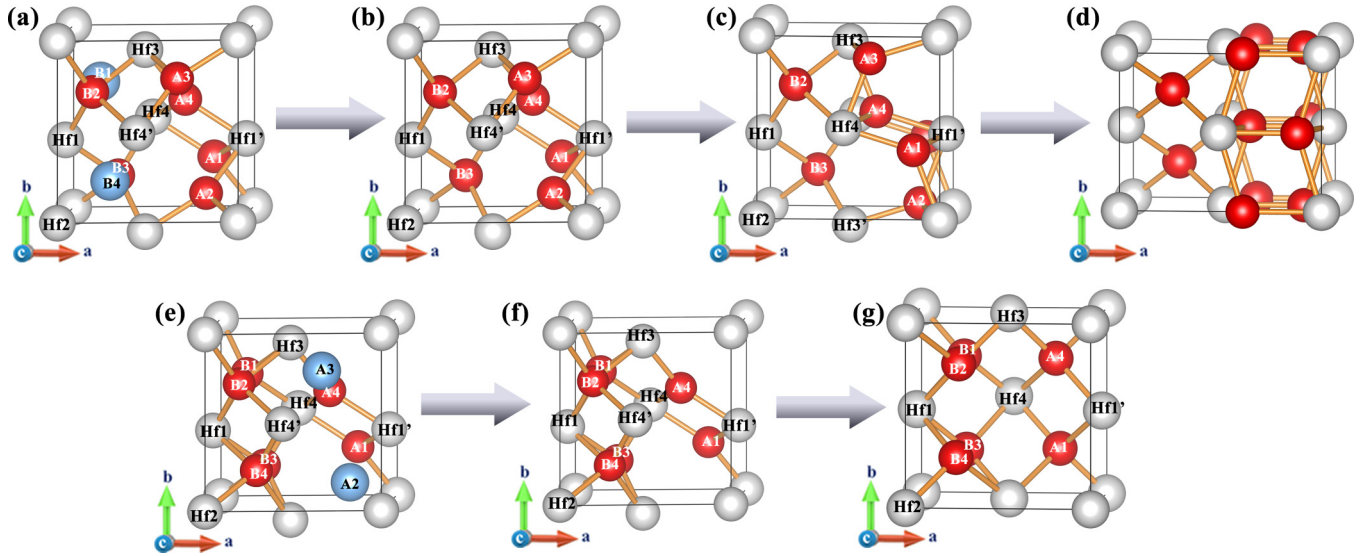


FIG. 7. The procedure of atomic structure evolution between (a)–(d)  $m\text{-HfO}_{1.5}$  and  $P4m2\text{-HfO}_{1.5}$ , and (e)–(g)  $m\text{-HfO}_{1.5}$  and  $P2/c\text{-HfO}_{1.5}$ .

previous experiments demonstrate that this range is between 100 kΩ and 3 MΩ for a hafnia-memristor with 20 nm dielectric thickness and 80 μm × 80 μm device area [63].

Although the conductivity of  $m\text{-HfO}_x$  varies monotonously with O content, the realization of multivalue storage and continuous conductivity modulation of  $m\text{-HfO}_x$  is seriously hindered by the mobile characteristics of  $V_O$ . As shown in Fig. 11(a), due to the poor symmetry of  $m\text{-HfO}_2$ , there are nine inequivalent  $V_O$  migration paths. Distinct from the analysis in Sec. III C 1, we only focus here on migration between neighbor sites, with any individual hopping distance limited to within 3 Å. This is because RS within  $m\text{-HfO}_x$  does not involve high driving force, but a phase transition requires drastic structural changes, such that the paths in Sec. III C 1 are all beyond 4 Å. For the sake of conductance modulation, the results in Fig. 11(b) show that  $V_O$  in  $m\text{-HfO}_2$  has the lowest migration barrier along Path-8 (1.72 eV). Moreover, continuous migration solely through Path-8 is possible, without invoking other paths. Therefore, CFs can preferably be created along this path in the  $c$ -axis direction. The  $V_O$  migration barriers for other paths lie between 2.26 and 3.00 eV. However, when electrons detrapp from a neutral  $V_O$  to generate charged  $V_O^{2+}$  under the applied electric field, the migration barrier of each path decreases significantly, and the migration barrier of Path-1 is as low as 0.34 eV. The migration barriers of Path-5, Path-6,

Path-8, and Path-9 are lower than 1.00 eV. These paths altogether cover migration in all directions, thus  $V_O^{2+}$  in  $m\text{-HfO}_2$  is prone to diffusion/drift, which will lead to instability of O content in CFs as well as poor stability and consistency of the HRS. Diffusion can be achieved along multiple paths with mixed directions. Therefore, it is difficult to achieve stable multivalue storage and continuous conductance modulation.

### 3. RS within $\gamma\text{-HfO}_x$

For  $1.0 < x < 1.5$ , there are phases that are derivatives of  $\gamma\text{-HfO}_{1.5}$  and  $\alpha\text{-HfO}_{1.5}$ , respectively. Conductive paths of  $\gamma\text{-HfO}_{1.5}$  composition have been observed in experiments [34], but CFs of  $\alpha\text{-HfO}_{1.5}$  composition have never been discovered in memristors. In addition, derivatives of  $\alpha\text{-HfO}_{1.5}$  can be regarded as derivatives of  $\gamma\text{-HfO}_{1.5}$  with more  $V_O$ 's (cf. Fig. 6). Therefore, these CF candidates will be globally referred to as  $\gamma\text{-HfO}_x$ . In the  $x$  range of interest, the structures and density of states of  $\gamma\text{-HfO}_x$  are shown in Fig. 12. Obviously, the density of states of  $\gamma\text{-HfO}_{1.5}$  is similar to that of  $m\text{-HfO}_{1.5}$ , and the defect states introduced by  $V_O$  are distributed below CBM. With the decrease of O content, the number of shallow defect states increases. For  $x < 1.25$ ,  $\gamma\text{-HfO}_x$  becomes metallic. The conductivity of  $\gamma\text{-HfO}_{1.5}$  is similar to that of  $m\text{-HfO}_{1.5}$ , which indicates that the change of CF structure from  $m\text{-HfO}_{1.5}$  to  $\gamma\text{-HfO}_{1.5}$  will not lead to the sudden change in the conductance of  $\text{HfO}_2$ -based memristor. In addi-

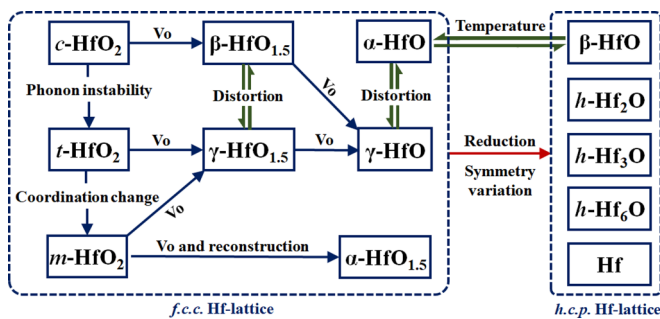


FIG. 8. Relation of intertransition between various Hf-O compounds during the reduction process of  $\text{HfO}_2$ .

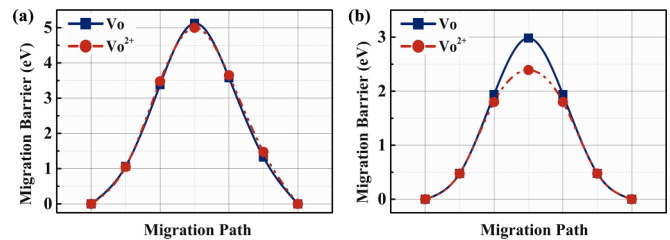


FIG. 9. The  $V_O$  and  $V_O^{2+}$  migration barriers in  $m\text{-HfO}_2$  under the paths of (a)  $B4 \rightarrow B1$  and (b)  $A2 \rightarrow A3$ .



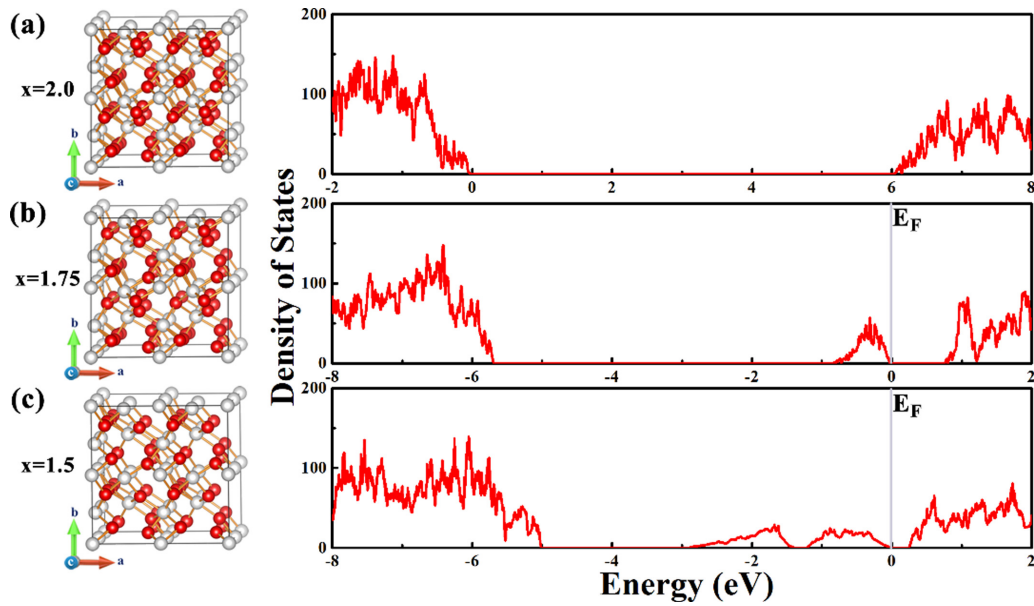


FIG. 10. The crystal structures and density of states of (a)  $m\text{-HfO}_2$ , (b)  $m\text{-HfO}_{1.75}$ , and (c)  $m\text{-HfO}_{1.5}$ . The Fermi levels ( $E_F$ ) are marked in (b) and (c).

tion, the phase-transition temperature between  $\gamma\text{-HfO}_{1.5}$  and  $m\text{-HfO}_{1.5}$  is estimated to be merely 62 K, and reversible transition may be realized in the practical operation process. Theoretically, when O content in CFs is maintained at  $1 < x < 2$ , hafnia-based memristor can realize continuous conductivity modulation with a large adjustable range (from an insulating state to a metallic state) by controlling the O content in CFs.

However, like  $m\text{-HfO}_x$ , the stability of  $V_O$  in  $\gamma\text{-HfO}_{1.5}$  is also poor. As shown in Fig. 13,  $V_O$  has only two inequivalent paths in  $\gamma\text{-HfO}_{1.5}$  due to its higher symmetry. The migration barriers of  $V_O$  along Path-1 and Path-2 are 0.83 and 1.22 eV, respectively, both lower than that in  $m\text{-HfO}_2$ . Therefore, CFs composed of  $\gamma\text{-HfO}_x$  still hardly provide stable low and intermediate resistance states for hafnia-based memristors. Different from the case of  $m\text{-HfO}_2$ , the migration barrier of  $V_O^{2+}$  (1.17 eV for Path-1 and 1.82 eV for Path-2) is higher than that of neutral  $V_O$ . The reason is analyzed as follows, considering  $m\text{-HfO}_2$  and  $\gamma\text{-HfO}_{1.5}$ . As shown in Fig. S2(a) of

Note 5 of the Supplemental Material [58], the defect states induced by a neutral  $V_O$  in  $m\text{-HfO}_2$  are spatially localized exactly at the  $V_O$  location. These electrons tend to block the migration of a negatively charged O anion to the vacancy site, thus causing a higher migration barrier of neutral  $V_O$  compared with  $V_O^{2+}$  in normal cases. Nevertheless, the trapped electrons only loosely surround the vacancy site in  $\gamma\text{-HfO}_{1.5}$ , as illustrated in Fig. S2(b) of Note 5 of the Supplemental Material [58], close to the Hf sites. These electrons do not hinder the transport of  $O^{2-}$ , thus accelerating the migration of neutral  $V_O$  in  $\gamma\text{-HfO}_{1.5}$ .

#### 4. RS involving $h\text{-HfO}_x$

The atomic structure and density of states of  $h\text{-HfO}_x$  under various O contents are shown in Fig. 14, all of which are strong metals and contain many interstitial positions for O. Among the highly reduced  $\text{HfO}_x$  phases with  $x < 1.0$ ,  $h\text{-Hf}_6\text{O}$

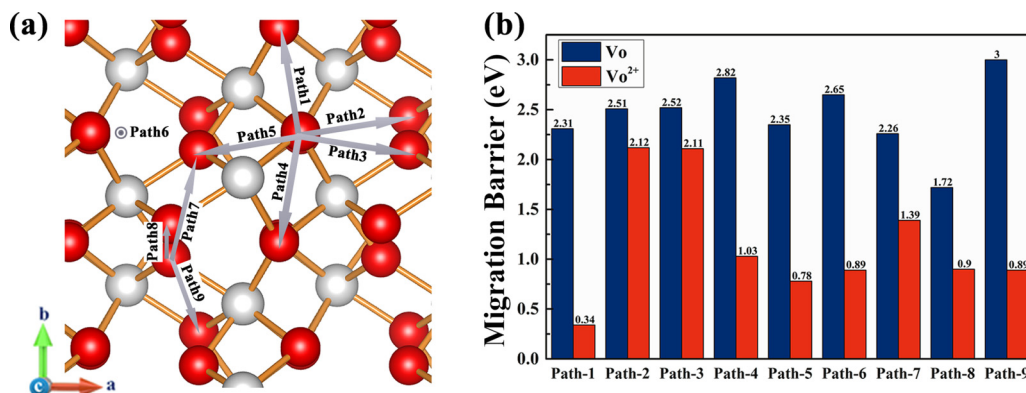


FIG. 11. (a) The schematic diagram of  $V_O$  migration path in  $m\text{-HfO}_2$ ; (b) the histogram of  $V_O$  migration barriers under different paths.

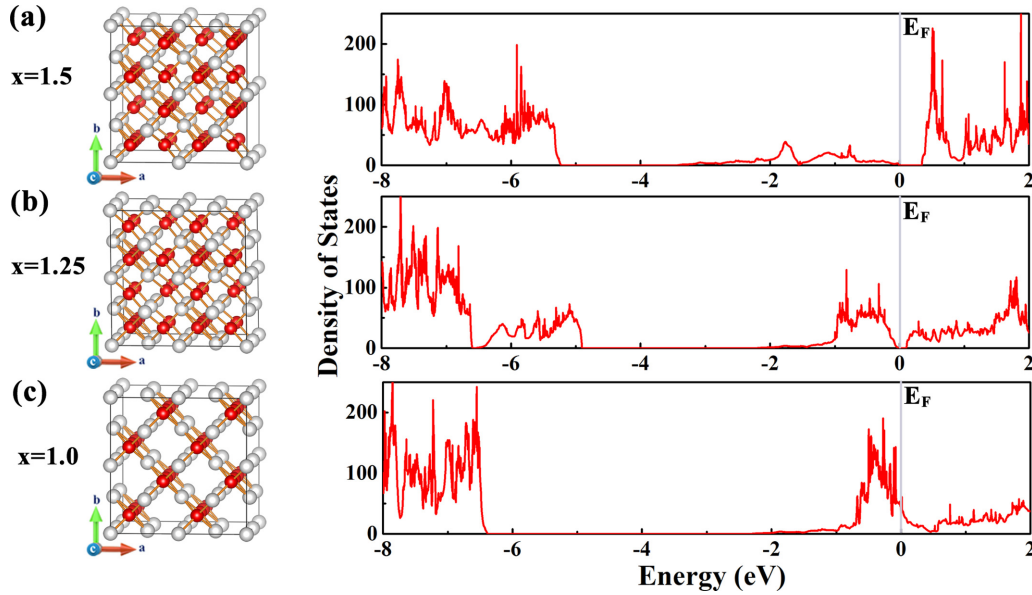


FIG. 12. The crystal structures and density of states of (a)  $\gamma$ -HfO<sub>1.5</sub>, (b)  $\gamma$ -HfO<sub>1.25</sub>, and (c)  $\gamma$ -HfO.

has been proved to be a stable phase at room temperature and normal pressure [41], whose hexagonal structure is shown in Fig. 14(d). CFs with the  $h$ -HfO <sub>$x$</sub>  composition clearly indicate a low resistance state (LRS) of the memristor, and  $h$ -Hf<sub>6</sub>O has been widely discovered as the CF composition in the experiment of Zhang *et al.* [34]. Similar to  $\alpha$ -HfO<sub>1.5</sub>,  $h$ -HfO <sub>$x$</sub>  requires absorbing a number of O atoms so as to be ruptured. The robust nature of  $h$ -HfO <sub>$x$</sub>  leads to violent SET/RESET processes, and hafnia memristors in this mode exhibit obvious sharp-transition binary characteristics.

Mao *et al.* carried out a comprehensive study on the migration barriers of O atoms in  $h$ -HfO <sub>$x$</sub>  under various O contents, giving barriers between 2.26 and 3.64 eV [46], significantly higher than in  $m$ -HfO<sub>1.5</sub> and  $\gamma$ -HfO<sub>1.5</sub>. This greatly strengthens the stability of the CF structure. On the other hand, the O content in  $h$ -HfO <sub>$x$</sub>  has little influence on its conductivity characteristics [46], rendering the LRS level robust if constructed from  $h$ -HfO <sub>$x$</sub> . Although multivalued storage and continuous conductance modulation can be realized by controlling the size of the CFs [64], CFs remain highly conductive, and the linearly adjustable range of conductance is limited [63].

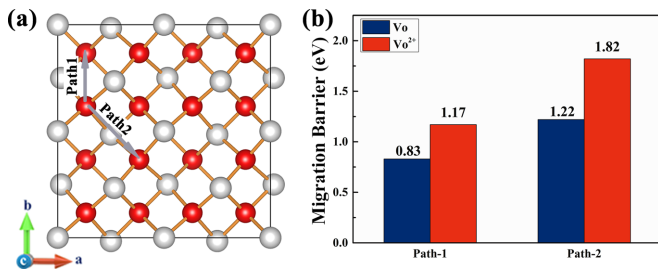


FIG. 13. (a) The schematic diagram of  $V_O$  migration path in  $P4_2/nmc$ -HfO<sub>1.5</sub>; (b) the histogram of  $V_O$  migration barriers under different paths.

#### D. The size effect of CFs

The above analysis implies that gradual conductance modulation is possible in hafnia memristors by restricting the CF composition to monoclinic or tetragonal phases, rather than incurring the highly reduced hexagonal phases. The modulation is ideally achieved through controlling the excitation barriers from the defective states. However, experimentally it is difficult to obtain a wide range of continuous conductance modulation in undoped hafnia [24,63,65–69]. In addition to the poor thermal stability of  $V_O$ 's, the CF size effect in  $m$ -HfO <sub>$x$</sub>  or  $\gamma$ -HfO <sub>$x$</sub>  compositions is another key factor, namely, to what dimension the CFs of  $m$ -HfO <sub>$x$</sub>  or  $\gamma$ -HfO <sub>$x$</sub>  structure can remain stable. According to thermodynamic data [34], a sufficiently large  $m$ -HfO <sub>$x$</sub>  or  $\gamma$ -HfO <sub>$x$</sub>  CF ( $1.0 < x < 2.0$ ) tends to decompose into  $m$ -HfO<sub>2</sub> and  $h$ -Hf<sub>6</sub>O, but small CFs of such compositions may become stable due to the established interfaces in their chemical environment. Therefore, this section is devoted to the stability of CF models consisting of  $m$ -HfO <sub>$x$</sub>  with various sizes [shown in Figs. 15(a)–15(c)], as well as CFs composed of  $h$ -HfO <sub>$x$</sub>  with the same  $V_O$  concentrations [shown in Figs. 15(d)–15(f)]. All CFs are embedded in a  $7 \times 1 \times 7$   $m$ -HfO<sub>2</sub> supercell. The construction of  $m$ -HfO <sub>$x$</sub>  CF models is straightforward so as to introduce a number of  $V_O$  chains in a given region of the  $7 \times 1 \times 7$   $m$ -HfO<sub>2</sub> supercell. A minimum distance is kept between vacancy chains to ensure a local stoichiometry of  $\sim$ HfO<sub>1.5</sub>, without collapsing into metal Hf-like phases. It is, however, more complicated to create  $h$ -HfO <sub>$x$</sub>  CFs inside  $m$ -HfO<sub>2</sub> because of the symmetry incompatibility. Here we carry out a two-step process. First, both Hf and O atoms are removed, in a 1:2 atomic ratio, from a certain region of the  $7 \times 1 \times 7$   $m$ -HfO<sub>2</sub> supercell. Subsequently, a size-matched  $h$ -Hf<sub>6</sub>O supercell is filled in this hollow region. The hexagonal structure of the CF is maintained as well as possible, and the number of  $V_O$ 's is kept the same as the corresponding  $m$ -HfO <sub>$x$</sub>  CF models ( $N_{V_O} = 2N_{Hf} - N_O$ ).

In Fig. 15, only those models with the same  $V_O$  content could be compared, i.e., (a) with (d), (b) with (e), and (c)

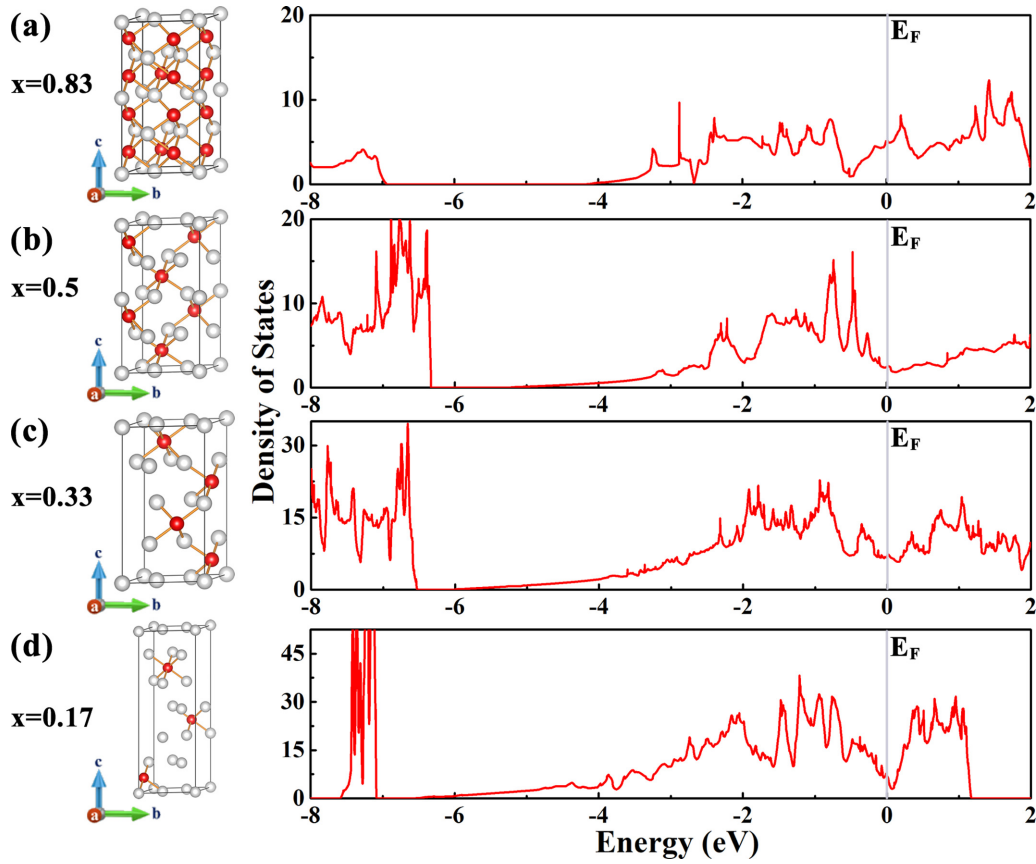


FIG. 14. The crystal structures and density of states of (a)  $h\text{-Hf}_6\text{O}_5$ , (b)  $h\text{-Hf}_2\text{O}$ , (c)  $h\text{-Hf}_3\text{O}$ , (d)  $h\text{-Hf}_6\text{O}$ .

with (f). Since the hexagonal phase can be regarded as a consequence of  $V_O$  aggregation, while in  $m\text{-HfO}_x$  the  $V_O$ 's are still apart from each other, we define here a cohesive energy of the  $V_O$  as

$$E_c = \frac{E_{h\text{-Hf}_6\text{O}} - E_{m\text{-HfO}_{1.5}}}{N_{V_O}}$$

where  $E_{h\text{-Hf}_6\text{O}}$  is the formation energy of  $h\text{-Hf}_6\text{O}$  CFs,  $E_{m\text{-HfO}_{1.5}}$  is the formation energy of  $m\text{-HfO}_{1.5}$  CFs, and  $N_{V_O}$  is the amount of  $V_O$  per supercell. The formation energy of a CF is

$$E_{\text{form}} = E_{\text{model}} + N_{V_O}\mu_O - nE_{\text{HfO}_2},$$

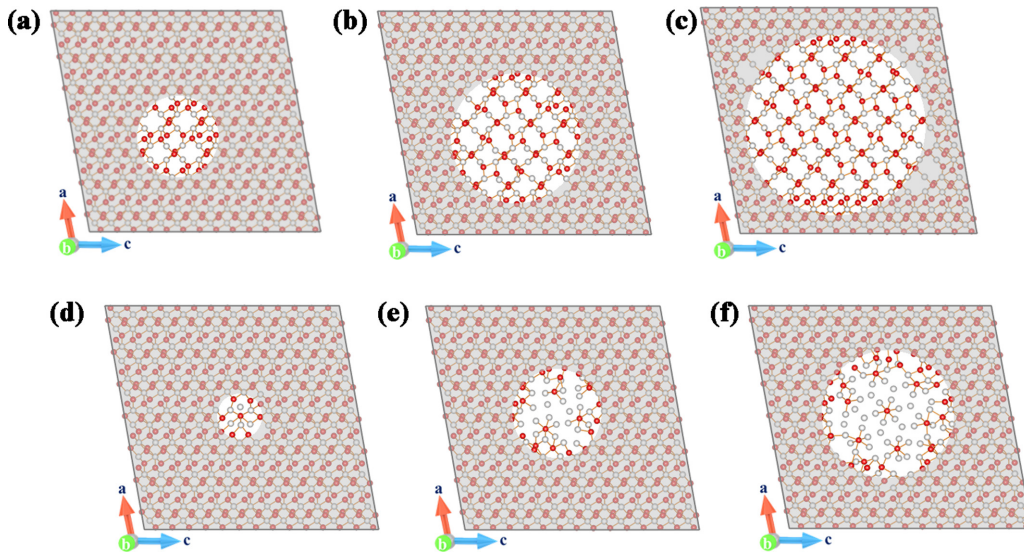


FIG. 15. Structural illustrations of various CF-in-dielectric models. CFs of  $m\text{-HfO}_{1.5}$  composition, with global  $V_O$  content at (a) 2.8%, (b) 11.2%, and (c) 25.3%; CFs of  $h\text{-Hf}_6\text{O}$  composition, with global  $V_O$  content at (d) 2.8%, (e) 11.2%, and (f) 25.3%. Dielectric regions outside the CF are faded to some extent to emphasize the CF location.

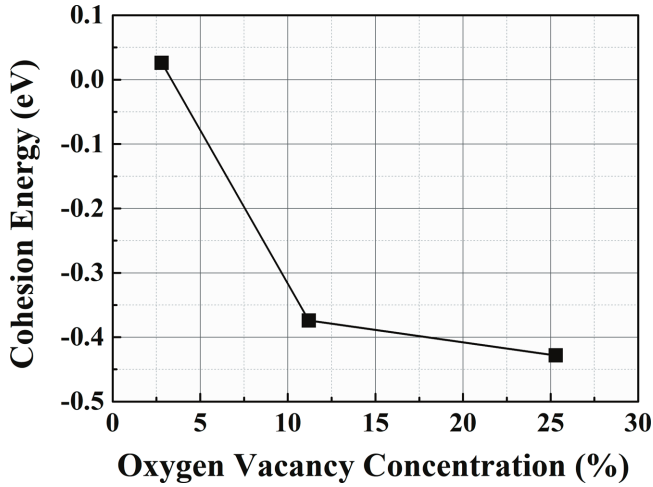


FIG. 16. The average cohesion energy of CFs in  $h\text{-Hf}_6\text{O}$  at various  $V_{\text{O}}$  contents.

where  $E_{\text{model}}$  is the energy after model relaxation,  $\mu_{\text{O}}$  is the chemical potential of the O element,  $E_{\text{HfO}_2}$  is the energy of ground state  $m\text{-HfO}_2$ , and  $n$  accounts for the size of the model supercell.

Therefore,  $E_c$  reflects the energy required for the CF structure to evolve from  $m\text{-HfO}_{1.5}$  to  $h\text{-Hf}_6\text{O}$  (see Fig. 16). When the  $V_{\text{O}}$  concentration is merely 2.8%, corresponding to  $\sim 1$  nm diameter of  $m\text{-HfO}_{1.5}$  CFs, the  $E_c$  value is positive (0.03 eV), indicating that  $m\text{-HfO}_{1.5}$  CFs are more stable. When the  $V_{\text{O}}$  concentration rises to 11.2% (the diameter of  $m\text{-HfO}_{1.5}$ -CFs reaching  $\sim 2$  nm),  $E_c$  decreases rapidly to a negative value  $-0.37$  eV, predicting a spontaneous transformation of the CF into  $h\text{-Hf}_6\text{O}$  structure. As the  $V_{\text{O}}$  concentration increases further,  $E_c$  does not change significantly, but still listing  $h\text{-Hf}_6\text{O}$  as the favorable CF composition. Hence, a CF composed of  $m\text{-HfO}_{1.5}$  would become unstable as its diameter exceeds 1 nm, collapsing to  $h\text{-Hf}_6\text{O}$ . Such a process is drastic as it involves sharp symmetry conversion and composition changes, which is related to the binary character of the RS.

### E. Connection to experimental research on hafnia-based memristors

In this section, we relate our theoretical outcomes to the existing experimental research. As it is well accepted that the chemical composition and defect concentration are highly relevant to the crystalline structure of  $\text{HfO}_x$  thin film as well as its RS characteristics, Kaiser *et al.* [47] recently investigated the crystal structures of  $\text{HfO}_x$  thin films throughout the entire stoichiometries, using x-ray diffraction (XRD), x-ray photoelectron spectroscopy (XPS), and HRTEM techniques. The results reveal that  $\text{HfO}_x$  transforms from monoclinic symmetry to a low-temperature phase  $c\text{-HfO}_{1.7}$  (LTP  $c\text{-HfO}_{1.7}$ ) as  $x$  decreases, which is maintained until  $x = 0.7$ . Subsequently, the structure becomes  $h\text{-HfO}_{0.7}$ . The LTP  $c\text{-HfO}_{1.7}$  phase is described as an oxygen defect-stabilized cubic phase, but it is shown that this phase has a slight distortion from the ideal cubic structure. The experimentally observed phase-transition procedure during the reduction of hafnia is consistent with

our theoretical results. Moreover, the structure of LTP  $c\text{-HfO}_x$  fits our definition of the fcc Hf-lattice, and its topology is similar to  $\gamma\text{-HfO}_x$  when the distortion from a cubic structure is considered [comparing Figs. 7(g) and 8 in Ref. [47]]. Moreover, our calculated electronic structures for various  $\text{HfO}_x$  phases show that the resistance of  $\text{HfO}_x$  may vary continuously with the oxygen content, enabling the possible analog memristor. Kaiser and co-workers measured the thin-film resistivity of  $\text{HfO}_x$  with various oxygen contents [47]. It follows that  $\text{HfO}_x$  is an insulator for  $x > 1.7$ , and the resistivity decreases continuously from  $\sim 10^{-4} \Omega\text{m}$  to  $\sim 7.3 \times 10^{-6} \Omega\text{m}$  as  $x$  varies from 1.7 to 0.7. This supports the argument of this work on the possible analog working mode of hafnia-based memristor.

On the other hand, Zhang *et al.* studied the evolution of CFs in hafnia memristors [34], showing that the rupture of  $h\text{-HfO}_x$  CFs renders the binary RS of the device, and the ruptured part of the partial CF is  $m\text{-HfO}_x$ . This evidence supports the scenario of the binary RS in hafnia as presented in this work. In addition, Zhang and co-workers identified the CF as in a core-shell structure, where  $h\text{-Hf}_6\text{O}$  conductive channels are surrounded by  $m\text{-HfO}_2$  (or sometimes  $t\text{-HfO}_2$ ) under TEM observation. The horizontal dimension of  $h\text{-Hf}_6\text{O}$  is typically  $\sim 10$  nm. Theoretically, the cohesive tendency of  $V_{\text{O}}$ 's indeed prefers the  $h\text{-Hf}_6\text{O}$  CF composition, as long as the SET/RESET voltages are not so constrained. This could explain the usually discovered binary RS characteristics in undoped hafnia.

When the SET and RESET operations are constrained, it is possible to achieve continuous conductance modulation in hafnia, but there are still two obstacles. On the one hand, the low and somehow isotropic migration barrier of  $V_{\text{O}}$  adds to the instability of the resistance levels of the HRS. On the other hand, the strong accumulation tendency of  $V_{\text{O}}$  and  $V_{\text{O}}$  chains [40] facilitates the formation of  $h\text{-Hf}_6\text{O}$  CFs, promoting the binary switching mode. Element doping is, however, a convenient and effective means to adjust the  $V_{\text{O}}$  migration kinetics in hafnia. In experimental research, dopants such as Al, Gd, Ni, and Zr are utilized to enhance the  $V_{\text{O}}$  migration barrier, leading to better uniformity and multilevel RS in hafnia [38,69–71]. These studies could verify the theoretical principles to some extent. Nevertheless, there are few works that consider overcoming the second obstacle, i.e., hindering the accumulation of  $V_{\text{O}}$ 's and the formation of the hexagonal structures. Very recently, we have reported the encouraging role of Mg doping in improving the resistance level stability in hafnia memristors [63]. Here we review the impact of Mg doping in terms of the migration barrier and  $V_{\text{O}}$  aggregation controls.

It is known that Mg tends to occupy interstitial locations in hafnia [72], where the favorite location is indicated by the orange atoms in Fig. 17. Our focus is the  $V_{\text{O}}$ 's surrounding an Mg dopant. Their migration barriers in several directions, as illustrated in Fig. 17, are summarized in Fig. 18. Compared with undoped hafnia, the migration barriers of  $V_{\text{O}}$  and  $V_{\text{O}}^{2+}$  near the Mg dopant have both increased dramatically, reaching 2.24–2.69 eV ( $V_{\text{O}}$ ) and 1.82–2.80 eV ( $V_{\text{O}}^{2+}$ ), respectively. This would improve the resistance level stability in hafnia, explaining the robust multilevel RS phenomena observed in  $\text{Mg:HfO}_x$  memristors [63]. On the other hand,

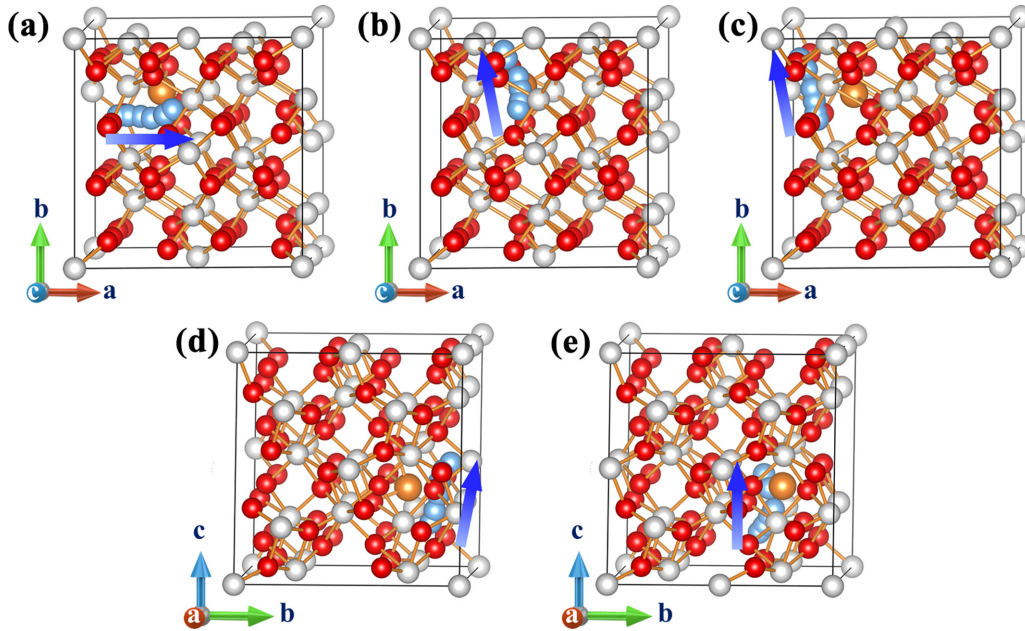


FIG. 17. Migration path diagrams of  $V_O$  near Mg dopant in various directions. The green balls plus the corresponding arrows indicate the paths.

$V_O^{2+}$  surrounding Mg tends to migrate along Path-b2 (1.82 eV barrier), but all other paths present barriers no less than 2.16 eV. Consequently, Mg doping introduces some anisotropy in  $V_O$  diffusion/migration, favoring the CFs along the direction of Path-b2. In other words, the horizontal migration from or into the CFs becomes relatively more difficult. To a certain extent, such anisotropic migration tends to hinder the merging of small CFs into a strong CF, delaying the possible phase transition into  $h$ - $Hf_6O$ . These two features are helpful for the memristor to work in the gradual conductance modulation mode, or analog mode. Similar theoretical analysis may also be used for other element doping in hafnia-based memristors.

#### IV. CONCLUSION

We have explored the rule of structural evolution in  $HfO_2$ -based memristors under the condition of memristor operation modes. The possibility of continuous and gradual conductance modulation is discussed for the sake of neuromorphic applications. The following conclusions can be drawn:

(i)  $HfO_x$  undergoes a transition from the monoclinic phase to tetragonal phases, and eventually to hexagonal phases during the reduction process in a memristor. The Hf subsystem remains in an fcc-like structure for  $1 < x < 2$ , and transitions between various suboxide phases in this regime can be achieved through O vacancy migration. The conductance modulation is gradual by controlling the density and energy level of defect states. However, the Hf subsystem tends to transform into an hcp-like structure for  $x < 1$ , and the rupture and reformation of hexagonal conductive filaments render abrupt binary switching characteristics.

(ii) The previously predicted  $P\bar{4}m2$ -phase  $Hf_2O_3$  is found to consist of an fcc-like Hf sublattice with half O anions located at the rocksalt sites but half O anions at the fluorite sites. The transition barrier from monoclinic  $HfO_2$  to  $P\bar{4}m2$ -phase  $Hf_2O_3$  is high under the memristor operating conditions. On the other hand, a defective  $Hf_2O_3$  phase derived by introducing O vacancies in  $P4_2/nmc$ - $HfO_2$  (i.e.,  $P2/c$ - $Hf_2O_3$ ) and another predicted  $Ibam$ - $Hf_2O_3$  phase are more likely to emerge in  $HfO_x$ -memristors.

(iii) The recently observed  $I4_1/amd$ -phase is the most stable structure for the HfO stoichiometry at room temperature, and is similar to a  $P4_2/nmc$ -HfO phase. Both derive from  $P4_2/nmc$ - $HfO_2$  through O vacancy introduction, which is possible in memristor operations. The  $P\bar{6}2m$  phase HfO can be transformed from or to  $I4_1/amd$ -HfO by the temperature effect, which sets up a bridge between fcc Hf-lattice and hcp

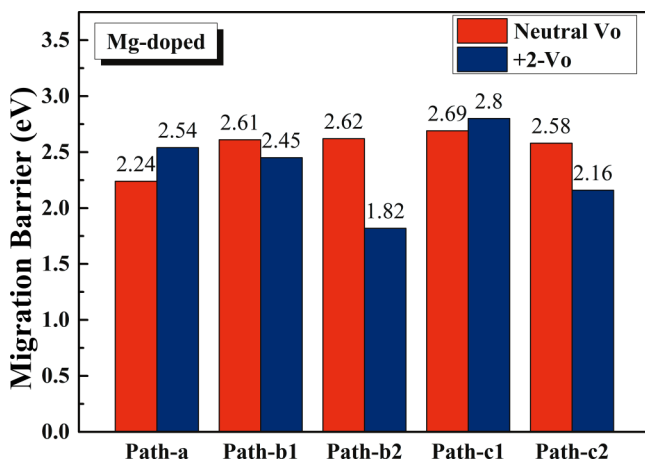


FIG. 18. Migration barriers of  $V_O$  and  $V_O^{2+}$  near an Mg dopant in different directions for Mg-doped hafnia memristor.

Hf-lattice. Nevertheless, such a transition cannot be achieved through a mild O vacancy migration process in a memristor environment. Hence, the resistive switching between Hf/Hf<sub>6</sub>O with hcp Hf-lattice and HfO<sub>x</sub> ( $x > 1$ ) with quasi-fcc Hf-lattice inevitably involves an abrupt transition.

(iv) The difficulty in obtaining gradual and robust conductance modulation in undoped HfO<sub>x</sub> lies in the fact that the migration of O vacancies in monoclinic or tetragonal HfO<sub>x</sub> structures is both fast and nearly isotropic, which facilitates the merging of O vacancies and O vacancy chains into strong filaments. Our calculation shows that strong filaments tend to

become hexagonal due to a phase transition at around  $x = 1$ , leading to typical binary switching characteristics. The effect of Mg doping is to introduce a certain degree of anisotropy in O vacancy diffusion/migration, which hinders the formation of hexagonal filaments, and thus stabilizes the mode of gradual conductance modulation.

#### ACKNOWLEDGMENTS

This work was supported by the National Key R&D Program of China under Grant No. 2019YFB2205100.

- 
- [1] S. Ginnaram, J. T. Qiu, and S. Maikap, Role of the Hf/Si interfacial layer on the high performance of MoS<sub>2</sub>-based conductive bridge RAM for artificial synapse application, *IEEE Electron Dev. Lett.* **41**, 709 (2020).
- [2] X. Hong, D. J. Loy, P. A. Dananjaya, F. Tan, C. Ng, and W. Lew, Oxide-based RRAM materials for neuromorphic computing, *J. Mater. Sci.* **53**, 8720 (2018).
- [3] S. Maikap and W. Banerjee, In quest of nonfilamentary switching: a synergistic approach of dual nanostructure engineering to improve the variability and reliability of resistive random-access-memory devices, *Adv. Electron. Mater.* **6**, 2000209 (2020).
- [4] B. Song, R. Cao, H. Xu, S. Liu, H. Liu, and Q. Li, A HfO<sub>2</sub>/SiTe based dual-layer selector device with minor threshold voltage variation, *Nanomaterials* **9**, 408 (2019).
- [5] D. Ielmini and H.-S. P. Wong, In-Memory computing with resistive switching devices, *Nat. Electron.* **1**, 333 (2018).
- [6] S. Balatti, S. Ambrogio, and D. Ielmini, Normally-off logic based on resistive switches—Part I: Logic gates, *IEEE Trans. Electron Dev.* **62**, 1831 (2015).
- [7] Z. Li, B. Tian, K.-H. Xue, B. Wang, M. Xu, H. Lu, H. Sun, and X. Miao, Coexistence of digital and analog resistive switching with low operation voltage in oxygen-gradient HfO<sub>x</sub> memristors, *IEEE Electron Dev. Lett.* **40**, 1068 (2019).
- [8] Z. Wang, M. Yin, T. Zhang, Y. Cai, Y. Wang, Y. Yang, and R. Huang, Engineering incremental resistive switching in TaO<sub>x</sub> based memristors for brain-inspired computing, *Nanoscale* **8**, 14015 (2016).
- [9] M. Mao, S. Yu, and C. Chakrabarti, Design and analysis of energy-efficient and reliable 3-D ReRAM cross-point array system, *IEEE Trans. VLSI Syst.* **26**, 1290 (2018).
- [10] A. Zaffora, D.-Y. Cho, K.-S. Lee, F. Di Quarto, R. Waser, M. Santamaria, and I. Valov, Electrochemical tantalum oxide for resistive switching memories, *Adv. Mater.* **29**, 1703357 (2017).
- [11] S. Choi, S. H. Tan, Z. Li, Y. Kim, C. Choi, P.-Y. Chen, H. Yeon, S. Yu, and J. Kim, SiGe epitaxial memory for neuromorphic computing with reproducible high performance based on engineered dislocations, *Nat. Mater.* **17**, 335 (2018).
- [12] W. Wan, R. Kubendran, C. Schaefer, S. B. Eryilmaz, W. Zhang, D. Wu, S. Deiss, P. Raina, H. Qian, B. Gao, S. Joshi, H. Wu, H.-S. P. Wong, and G. Cauwenberghs, A compute-in-memory chip based on resistive random-access memory, *Nature* **608**, 504 (2022).
- [13] P.-H. Chen, K.-C. Chang, T.-C. Chang, T.-M. Tsai, C.-H. Pan, T.-J. Chu, M.-C. Chen, H.-C. Huang, I. Lo, J.-C. Zheng, and S. M. Sze, Bulk oxygen-ion storage in indium-tin-oxide electrode for improved performance of HfO<sub>2</sub>-based resistive random access memory, *IEEE Electron Dev. Lett.* **37**, 280 (2016).
- [14] Y. Li, K.-S. Yin, M.-Y. Zhang, L. Cheng, K. Lu, S.-B. Long, Y. Zhou, Z. Wang, K.-H. Xue, M. Liu, and X.-S. Miao, Correlation analysis between the current fluctuation characteristics and the conductive filament morphology of HfO<sub>2</sub>-based memristor, *Appl. Phys. Lett.* **111**, 213505 (2017).
- [15] Y. Wang, Qi Liu, S. Long, W. Wang, Q. Wang, M. Zhang, S. Zhang, Y. Li, Q. Zuo, J. Yang, and M. Liu, Investigation of resistive switching in Cu-doped HfO<sub>2</sub> thin film for multilevel non-volatile memory applications, *Nanotechnology* **21**, 045202 (2010).
- [16] T.-M. Tsai, C.-H. Wu, K.-C. Chang, C.-H. Pan, P.-H. Chen, N.-K. Lin, J.-C. Lin, Y.-S. Lin, W.-C. Chen, H. Wu, N. Deng, and H. Qian, Controlling the degree of forming soft-breakdown and producing superior endurance performance by inserting bn-based layers in resistive random access memory, *IEEE Electron Dev. Lett.* **38**, 445 (2017).
- [17] D. Acharyya, A. Hazra, and P. Bhattacharyya, A journey towards reliability improvement of TiO<sub>2</sub> based resistive random access memory: A review, *Microelectron. Reliab.* **54**, 541 (2014).
- [18] A. Prakash, J. Park, J. Song, J. Woo, E.-J. Cha, and H. Hwang, Demonstration of low power 3-Bit multilevel cell characteristics in aTaO<sub>x</sub>-Based RRAM by stack engineering, *IEEE Electron Dev. Lett.* **36**, 32 (2015).
- [19] L. Zhao, H.-Y. Chen, S.-C. Wu, Z. Jiang, S. Yu, T.-H. Hou, H.-S. P. Wong, and Y. Nishi, Multi-Level control of conductive nanofilament evolution in HfO<sub>2</sub> ReRAM by pulse-train operations, *Nanoscale* **6**, 5698 (2014).
- [20] L. Yang, C. Kuegeler, K. Szot, A. Ruediger, and R. Waser, The influence of copper top electrodes on the resistive switching effect in TiO<sub>2</sub> thin films studied by conductive atomic force microscopy, *Appl. Phys. Lett.* **95**, 013109 (2009).
- [21] F. Zahoor, T. Z. Azni Zulkifli, and F. A. Khanday, Resistive random access memory (RRAM): An overview of materials, switching mechanism, performance, multilevel cell (Mlc) storage, modeling, and applications, *Nanoscale Res. Lett.* **15**, 90 (2020).

- [22] Z.-H. Wu, K.-H. Xue, and X.-S. Miao, Filament-to-dielectric band alignments in  $\text{TiO}_2$  and  $\text{HfO}_2$  resistive rams, *J. Comput. Electron.* **16**, 1057 (2017).
- [23] K. Moon, M. Kwak, J. Park, D. Lee, and H. Hwang, Improved conductance linearity and conductance ratio of 1T2R synapse device for neuromorphic systems, *IEEE Electron Dev. Lett.* **38**, 1023 (2017).
- [24] W. He, H. Sun, Y. Zhou, K. Lu, K. Xue, and X. Miao, Customized binary and multi-level  $\text{HfO}_{2-x}$ -based memristors tuned by oxidation conditions, *Sci. Rep.* **7**, 10070 (2017).
- [25] T. Kim, H. Kim, J. Kim, and J.-J. Kim, Input voltage mapping optimized for resistive memory-based deep neural network hardware, *IEEE Electron Dev. Lett.* **38**, 1228 (2017).
- [26] P. Huang, X. Y. Liu, B. Chen, H. T. Li, Y. J. Wang, Y. X. Deng, K. L. Wei, L. Zeng, B. Gao, G. Du, X. Zhang, and J. F. Kang, A physics-based compact model of metal-oxide-based RRAM DC and AC operations, *IEEE Trans. Electron Dev.* **60**, 4090 (2013).
- [27] S. Brivio, J. Frascaroli, and S. Spiga, Role of metal-oxide interfaces in the multiple resistance switching regimes of Pt/ $\text{HfO}_2$ /TiN devices, *Appl. Phys. Lett.* **107**, 023504 (2015).
- [28] U. Celano, L. Goux, R. Degraeve, A. Fantini, O. Richard, H. Bender, M. Jurczak, and W. Vandervorst, Imaging the three-dimensional conductive channel in filamentary-based oxide resistive switching memory, *Nano Lett.* **15**, 7970 (2015).
- [29] S. Kumar, Z. Wang, X. Huang, N. Kumari, N. Davila, J. P. Strachan, D. Vine, A. L. D. Kilcoyne, Y. Nishi, and R. S. Williams, Conduction channel formation and dissolution due to oxygen thermophoresis/diffusion in hafnium oxide memristors, *ACS Nano* **10**, 11205 (2016).
- [30] Y. Yang, X. Zhang, L. Qin, Q. Zeng, X. Qiu, and R. Huang, Probing nanoscale oxygen ion motion in memristive systems, *Nat. Commun.* **8**, 15173 (2017).
- [31] J. Yin, F. Zeng, Q. Wan, F. Li, Y. Sun, Y. Hu, J. Liu, G. Li, and F. Pan, Adaptive crystallite kinetics in homogenous bilayer oxide memristor for emulating diverse synaptic plasticity, *Adv. Funct. Mater.* **28**, 1706927 (2018).
- [32] G. Bersuker, D. C. Gilmer, D. Veksler, P. Kirsch, L. Vandelli, A. Padovani, L. Larcher, K. McKenna, A. Shluger, V. Iglesias *et al.*, Metal oxide resistive memory switching mechanism based on conductive filament properties, *J. Appl. Phys.* **110**, 124518 (2011).
- [33] K.-H. Xue, P. Blaise, L. R. C. Fonseca, G. Molas, E. Vianello, B. Traoré, B. De Salvo, G. Ghibaudo, and Y. Nishi, Grain boundary composition and conduction in  $\text{HfO}_2$ : An ab initio study, *Appl. Phys. Lett.* **102**, 201908 (2013).
- [34] Y. Zhang, G.-Q. Mao, X. Zhao, Y. Li, M. Zhang, Z. Wu, W. Wu, H. Sun, Y. Guo, L. Wang, X. Zhang, Q. Liu, H. Lv, K.-H. Xue, G. Xu, X. Miao, S. Long, and M. Liu, Evolution of the conductive filament system in  $\text{HfO}_2$ -Based memristors observed by direct atomic-scale imaging, *Nat. Commun.* **12**, 7232 (2021).
- [35] K. P. McKenna, Optimal stoichiometry for nucleation and growth of conductive filaments in  $\text{HfO}_x$ , *Model. Simul. Mater. Sci. Eng.* **22**, 025001 (2014).
- [36] T. V. Perevalov and D. R. Islamov, Atomic and electronic structures of the native defects responsible for the resistive effect in  $\text{HfO}_2$ : Ab initio simulations, *Microelectron. Eng.* **216**, 111038 (2019).
- [37] Y. Dai, Z. Pan, F. Wang, and X. Li, Oxygen vacancy effects in  $\text{HfO}_2$ -based resistive switching Memory: First principle study, *AIP Adv.* **6**, 085209 (2016).
- [38] F. Xu, B. Gao, Y. Xi, J. Tang, H. Wu, and H. Qian, Atomic-device hybrid modeling of relaxation effect in analog RRAM for neuromorphic computing, in *2020 IEEE International Electron Devices Meeting (IEDM)* (IEEE, San Francisco, 2020), pp. 13.2.1–13.2.4.
- [39] L. Sementa, L. Larcher, G. Barcaro, and M. Montorsi, Ab initio modelling of oxygen vacancy arrangement in highly defective  $\text{HfO}_2$  resistive layers, *Phys. Chem. Chem. Phys.* **19**, 11318 (2017).
- [40] K.-H. Xue and X.-S. Miao, Oxygen vacancy chain and conductive filament formation in hafnia, *J. Appl. Phys.* **123**, 161505 (2018).
- [41] J. Zhang, A. R. Oganov, X. Li, K.-H. Xue, Z. Wang, and H. Dong, Pressure-induced novel compounds in the Hf-O system from first-principles calculations, *Phys. Rev. B* **92**, 184104 (2015).
- [42] B. Puchala and A. Van der Ven, Thermodynamics of the Zr-O system from first-principles calculations, *Phys. Rev. B* **88**, 094108 (2013).
- [43] K.-H. Xue, B. Traore, P. Blaise, L. R. C. Fonseca, E. Vianello, G. Molas, B. De Salvo, G. Ghibaudo, B. Magyari-Kope, and Y. Nishi, A combined ab initio and experimental study on the nature of conductive filaments in Pt/ $\text{HfO}_2$ /Pt resistive random access memory, *IEEE Trans. Electron Dev.* **61**, 1394 (2014).
- [44] K.-H. Xue, P. Blaise, L. R. C. Fonseca, and Y. Nishi, Prediction of Semimetallic Tetragonal  $\text{Hf}_2\text{O}_3$  and  $\text{Zr}_2\text{O}_3$  from First Principles, *Phys. Rev. Lett.* **110**, 065502 (2013).
- [45] K. Z. Rushchanskii, S. Blügel, and M. Ležaić, Routes for increasing endurance and retention in  $\text{HfO}_2$ -based resistive switching memories, *Phys. Rev. Materials* **2**, 115002 (2018).
- [46] G.-Q. Mao, K.-H. Xue, Y.-Q. Song, W. Wu, J.-H. Yuan, L.-H. Li, H. Sun, S. Long, and X.-S. Miao, Oxygen migration around the filament region in  $\text{HfO}_x$  memristors, *AIP Adv.* **9**, 105007 (2019).
- [47] N. Kaiser, T. Vogel, A. Zintler, S. Petzold, A. Arzumanov, E. Piros, R. Eilhardt, L. Molina-Luna, and L. Alff, Defect-stabilized substoichiometric polymorphs of hafnium oxide with semiconducting properties, *ACS Appl. Mater. Inter.* **14**, 1290 (2022).
- [48] X. Luo, W. Zhou, S. V. Ushakov, A. Navrotsky, and A. A. Demkov, Monoclinic to tetragonal transformations in hafnia and zirconia: A combined calorimetric and density functional study, *Phys. Rev. B* **80**, 134119 (2009).
- [49] P. Hohenberg and W. Kohn, Inhomogeneous electron gas, *Phys. Rev.* **136**, B864 (1964).
- [50] W. Kohn and L. J. Sham, Self-consistent equations including exchange and correlation effects, *Phys. Rev.* **140**, A1133 (1965).
- [51] G. Kresse and J. Furthmüller, Efficiency of ab-initio total energy calculations for metals and semiconductors using a plane-wave basis set, *Comput. Mater. Sci.* **6**, 15 (1996).
- [52] G. Kresse and J. Furthmüller, Efficient iterative schemes for ab initio total-energy calculations using a plane-wave basis set, *Phys. Rev. B* **54**, 11169 (1996).
- [53] J. P. Perdew, K. Burke, and M. Ernzerhof, Generalized Gradient Approximation Made Simple, *Phys. Rev. Lett.* **77**, 3865 (1996).
- [54] L. G. Ferreira, M. Marques, and L. K. Teles, Approximation to density functional theory for the calculation of band gaps of semiconductors, *Phys. Rev. B* **78**, 125116 (2008).

- [55] G.-Q. Mao, Z.-Y. Yan, K.-H. Xue, Z. Ai, S. Yang, H. Cui, J.-H. Yuan, T.-L. Ren, and X. Miao, DFT-1/2 and shell DFT-1/2 methods: electronic structure calculation for semiconductors at LDA complexity, *J. Phys. Condens. Matter* **34**, 403001 (2022).
- [56] J.-H. Yuan, Q. Chen, L. R. C. Fonseca, M. Xu, K.-H. Xue, and X.-S. Miao, GGA-1/2 self-energy correction for accurate band structure calculations: The case of resistive switching oxides, *J. Phys. Commun.* **2**, 105005 (2018).
- [57] K.-H. Xue, J.-H. Yuan, L. R. C. Fonseca, and X.-S. Miao, Improved LDA-1/2 method for band structure calculations in covalent semiconductors, *Comput. Mater. Sci.* **153**, 493 (2018).
- [58] See Supplemental Material at <http://link.aps.org/supplemental/10.1103/PhysRevMaterials.6.084603> for more computational details and results.
- [59] L. Zhu, J. Zhou, Z. Guo, and Z. Sun, Metal-metal bonding stabilized ground state structure of early transition metal monoxide TM-MO (TM = Ti, Hf, V, Ta), *J. Phys. Chem. C* **120**, 10009 (2016).
- [60] J.-H. Yuan, G.-Q. Mao, K.-H. Xue, N. Bai, C. Wang, Y. Cheng, H. Lyu, H. Sun, X. Wang, and X. Miao, Ferroelectricity in HfO<sub>2</sub> from a chemical perspective, [arXiv:2201.00210](https://arxiv.org/abs/2201.00210).
- [61] E. Hildebrandt, J. Kurian, M. M. Müller, T. Schroeder, H.-J. Kleebe, and L. Alff, Controlled oxygen vacancy induced p-type conductivity in HfO<sub>2-x</sub> thin films, *Appl. Phys. Lett.* **99**, 112902 (2011).
- [62] R. R. Manory, T. Mori, I. Shimizu, S. Miyake, and G. Kimmel, Growth and structure control of HfO<sub>2-x</sub> films with cubic and tetragonal structures obtained by ion beam assisted deposition, *J. Vac. Sci. Technol. A* **20**, 549 (2002).
- [63] L.-H. Li, K.-H. Xue, L.-Q. Zou, J.-H. Yuan, H. Sun, and X. Miao, Multilevel switching in Mg-doped HfO<sub>x</sub> memristor through the mutual-ion effect, *Appl. Phys. Lett.* **119**, 153505 (2021).
- [64] S.-M. Park, H.-G. Hwang, J.-U. Woo, W.-H. Lee, S.-J. Chae, and S. Nahm, Improvement of conductance modulation linearity in a Cu<sup>2+</sup>-doped KNbO<sub>3</sub> memristor through the increase of the number of oxygen vacancies, *ACS Appl. Mater. Inter.* **12**, 1069 (2020).
- [65] S. Chandrasekaran, F. M. Simanjuntak, R. Saminathan, D. Panda, and T.-Y. Tseng, Improving linearity by introducing Al in HfO<sub>2</sub> as a memristor synapse device, *Nanotechnology* **30**, 445205 (2019).
- [66] B. Gao, L. Liu, and J. Kang, Investigation of the synaptic device based on the resistive switching behavior in hafnium oxide, *Progr. Nat. Sci.: Mater. Int.* **25**, 47 (2015).
- [67] S. Kim, Engineering synaptic characteristics of TaO<sub>x</sub>/HfO<sub>2</sub> bilayered resistive switching device, *Nanotechnology* **29**, 415204 (2018).
- [68] S. Kim, J. Chen, Y.-C. Chen, M.-H. Kim, H. Kim, M.-W. Kwon, S. Hwang, M. Ismail, Y. Li, X.-S. Miao *et al.*, Neuronal dynamics in HfO<sub>x</sub>/AlO<sub>y</sub>-based homeothermic synaptic memristors with low-power and homogeneous resistive switching, *Nanoscale* **11**, 237 (2019).
- [69] S. Roy, G. Niu, Q. Wang, Y. Wang, Y. Zhang, H. Wu, S. Zhai, P. Shi, S. Song, Z. Song *et al.*, Toward a reliable synaptic simulation using al-doped HfO<sub>2</sub> RRAM, *ACS Appl. Mater. Inter.* **12**, 10648 (2020).
- [70] H. Zhang, L. Liu, B. Gao, Y. Qiu, X. Liu, J. Lu, R. Han, J. Kang, and B. Yu, Gd-doping effect on performance of HfO<sub>2</sub> based resistive switching memory devices using implantation approach, *Appl. Phys. Lett.* **98**, 042105 (2011).
- [71] T. Tan, Y. Du, A. Cao, Y. Sun, G. Zha, H. Lei, and X. Zheng, The resistive switching characteristics of Ni-doped HfO<sub>x</sub> film and its application as a synapse, *J. Alloy. Compd.* **766**, 918 (2018).
- [72] D. Duncan, B. Magyari-Köpe, and Y. Nishi, Properties of Dopants in HfO<sub>x</sub> for Improving the Performance of Nonvolatile Memory, *Phys. Rev. Applied* **7**, 034020 (2017).